KeAi

CHINESE ROOTS
GLOBAL IMPACT

#### Contents lists available at ScienceDirect

# Petroleum Science

journal homepage: www.keaipublishing.com/en/journals/petroleum-science



# Original Paper

# Occurrence state of lacustrine shale oil in the second member of the Paleogene Kongdian Formation, Cangdong Sag, Bohai Bay Basin



Zhi-Hao Wang <sup>a,b</sup>, Jian-Hua Zhao <sup>a,b,\*</sup>, Xian-Zheng Zhao <sup>c</sup>, Ke-Yu Liu <sup>a,b</sup>, Xiu-Gang Pu <sup>c</sup>, Qin-Hong Hu <sup>a,b</sup>, Wen-Zhong Han <sup>c</sup>, Wei Zhang <sup>c</sup>, Zhan-Nan Shi <sup>c</sup>

- <sup>a</sup> State Key Laboratory of Deep Oil and Gas, China University of Petroleum (East China), Qingdao, 266580, Shandong, China
- <sup>b</sup> School of Geosciences, China University of Petroleum (East China), Qingdao, 266580, Shandong, China

#### ARTICLE INFO

#### Article history: Received 8 September 2024 Received in revised form 29 May 2025 Accepted 1 July 2025 Available online 7 July 2025

Edited by Jie Hao

Keywords: Shale oil occurrence state Controlling factors Multi-step programmed pyrolysis Cangdong Sag

#### ABSTRACT

Understanding the occurrence state of shale oil is crucial for the effective development of shale oil resources. Although the second member of the Kongdian Formation (Ek2) is a key interval for lacustrine shale oil production in the Cangdong Sag, Bohai Bay Basin, the occurrence state and controlling factors of shale oil in this formation remain poorly understood. This study established a multi-step programmed pyrolysis, combined with a light hydrocarbon recovery scheme, to quantitatively characterize the shale oil in different occurrence states. An integrated approach utilizing Rock-Eval pyrolysis, pyrolysis-gas chromatography, and crude oil gas chromatography was employed. Factors influencing the shale oil occurrence state were analyzed from petrology and organic geochemistry perspectives. The study revealed significant variations of shale oil occurrence states within the Ek2, attributed to differences in sedimentary organic matter, mineral compositions, sedimentary structures, and thermal maturity. Felsic laminae are the primary reservoir space for oil in laminated shales, and the frequent interbedding of felsic and organic-rich laminae facilitates the retention of free oil. The contents of free and adsorbed oil are primarily influenced by organic matter content and shale storage capacity, both of which exhibit distinct occurrence patterns. Based on the shale reservoir quality classification using the pyrolysis values of  $S_{1-1} + S_{1-2}$  and  $(S_{1-1} + S_{1-2}) \times 100/TOC$ , the Ek<sub>2</sub> shale demonstrates significant exploitation potential, with the first-level reservoirs comprising 66%, second-level reservoirs 11%, and third-level reservoirs 23%. These findings provide new insights into the geological accumulation and production of shale oil.

© 2025 The Authors. Publishing services by Elsevier B.V. on behalf of KeAi Communications Co. Ltd. This is an open access article under the CC BY-NC-ND license (http://creativecommons.org/licenses/by-nc-nd/4.0/).

# 1. Introduction

Shale oil exploration has significantly progressed in China, with an estimated resource potential of 200.88 billion tons (Jin et al., 2021a). However, unlike the successful development of marine shale oil in the U.S. (Sonnenberg and Pramudito, 2009; Rasdi and Chu, 2012; Centurion et al., 2013), Chinese shale oil production per well has experienced a rapid decline over time, rendering it economically unviable (Jin et al., 2021b; Lu et al., 2016). A major

Shale oil occurs in free, adsorbed, solution, and swelling states (Jarvie, 2012; Zou et al., 2013). Several methods have been proposed for distinguishing and quantifying different shale oil states, including the adsorption proportion equation, molecular simulation, multi-step solvent extraction, adsorption retention experiments, nuclear magnetic resonance, and Rock-Eval pyrolysis (Peters, 1986; Ambrose et al., 2012; Collell et al., 2014; Fleury and Romero-Sarmiento, 2016; Qian et al., 2017; Romero-Sarmiento, 2019). Rock-Eval pyrolysis is a rapid evaluation technique based

Peer review under the responsibility of China University of Petroleum (Beijing).

<sup>&</sup>lt;sup>c</sup> PetroChina Dagang Oilfield Company, Tianjin, 300280, China

reason for this phenomenon is the strong heterogeneity and the complex oil occurrence state in lacustrine shale reservoirs (Katz and Lin, 2014). Therefore, characterizing the occurrence states, movable oil content, and potentially recoverable shale oil reserves is crucial for identifying favorable exploration areas and developing effective development plans.

<sup>\*</sup> Corresponding author.

E-mail address: zhaojh@upc.edu.cn (J.-H. Zhao).

on the differences in molecular thermal volatilization of shale oil in different occurrence states (Espitalie et al., 1986; Peters, 1986; Behar et al., 1997; Maende et al., 2017; Romero-Sarmiento et al., 2014). Most of previous works have primarily focused on the classical S<sub>1</sub> peak obtained through Basic/Bulk-Rock parameters (Espitalie et al., 1977, 1986; Peters, 1986), However, several guestions still remain, such as whether the classical S<sub>1</sub> parameter and the corresponding extrapolation are reliable and significant for the geological conditions (Inan et al., 1998; Jarvie, 2012). To obtain a better assessment of these retained hydrocarbons in liquid-rich sedimentary rock, a specific pyrolysis program (Sh0-Sh2) for characterization of free versus adsorbed hydrocarbons was developed (Romero-Sarmiento et al., 2014, 2016; Romero-Sarmiento, 2019). However, little work has done to understand the oil/bitumen in Sh0 and Sh1 peaks compared to producible oil. Jiang et al. (2016) used a multi-step programmed pyrolysis with temperatures at 200, 350, 450, and 600 °C, providing information on occurrence state of shale oil, S<sub>1-1</sub> (practical movable oil content),  $S_{1-1} + S_{1-2}$  (maximum movable oil content),  $S_{2-1}$  (adsorbed oil content), and S<sub>2-2</sub> (hydrocarbon generated by kerogen), which is widely used to study shale oil occurrence state in China (Wang et al., 2019; Zhang et al., 2022). However, there are differences in the thermal volatilities of different components and the initial thermal cracking temperatures of maceral components (Teerman and Hwang, 1991; Lu, 1996; Romero-Sarmiento et al., 2016; Ko et al., 2018). Therefore, for shales with different kerogen types, differences in the multi-step programmed pyrolysis scheme should be considered to study the oil occurrence state. Furthermore, light hydrocarbons are easily volatilized during sample storage and preparation (Cooles et al., 1986; Michael et al., 2013; Beti et al., 2020), and approximately 30%-50% of these components can be lost (Cooles et al., 1986; Ma et al., 2005; Michael et al., 2013). Therefore, recovery of light hydrocarbon components is necessary during the quantitative characterization of shale oil content (Beti et al., 2020). Currently, the most widely used recovery methods are hydrocarbon generation kinetics and sealed coring methods (Lu, 1996; Ma et al., 2005). However, the hydrocarbon generation kinetics method is based on the hypothesis that all hydrocarbons are formed from in situ organic matter and it does not consider the effect of oil migration from adjacent intervals (Li et al., 2016). Although the sealed coring method is efficient, it is extremely expensive to be used widely.

TOC content is an important factor controlling hydrocarbon generation potential and oil content in shale (Sandvik et al., 1992; Michael et al., 2013; Wang et al., 2019; Feng et al., 2021). Previous works have established standards of reservoir evaluation. For instance, Jarvie (2012) posited that a shale oil reservoir holds exploitation potential only when the oil saturation index (OSI =  $S_1 \times 100/TOC$ ) reaches approximately 100 mg HC/g TOC. Lu et al. (2012) classified shale oil into three resource levels based on the triple-division characteristic between oil and TOC contents in source rock: scattered (ineffective), low efficient, and enriched resources. With advancements in experimental methods, evaluation standards have evolved accordingly. Romero-Sarmiento et al. (2017) proposed a modified oil saturation index [OSI =  $(Sh0 + Sh1) \times 100/TOC]$  based on the multi-step programmed pyrolysis. It is evident that updating experimental schemes and refining reservoir evaluation criteria are crucial for shale oil reservoir exploration and development.

The Ek<sub>2</sub> interval is significant for shale oil production in the Cangdong Sag, Bohai Bay Basin (Zhao et al., 2019). In order to quantitatively characterize shale oil in different occurrence states, pyrolysis-gas chromatography was employed to analyze thermal extracts across various temperature ranges. The multi-step programmed pyrolysis scheme can be established by analyzing the

compositions of crude oil and thermal extracts at various temperature ranges. The recovery coefficient of light hydrocarbon components can be determined by comparing the compositions of movable hydrocarbons with that of the crude oil. Additionally, factors influencing shale oil occurrence state and evaluation standards were investigated through a combining petrology and organic geochemistry analyses. This study enhances understanding of occurrence state of lacustrine shale oil and presents a practical method for optimizing the utilization of Rock-Eval pyrolysis testing to identify favorable targets for shale oil exploration.

#### 2. Geological setting

The Bohai Bay Basin, situated on the eastern coast of China, is a rhomboid-shaped basin covering approximately 200,000 km². It developed during the Mesozoic and Cenozoic periods, forming six depressions: Liaohe, Jizhong, Huanghua, Bozhong, Jiyang, and Linqing (Zhao et al., 2024). The Cangdong Sag, categorized as a secondary tectonic unit within the Huanghua Depression, lies to the south of it and is surrounded by the Xuhei, Kongdian, Dongguang, and Cangxian uplifts (Fig. 1). It has a linear configuration with a northeast to southwesterly strike, covering a total area of 1760 km² (Zhao et al., 2019). Originating as an early down-warped lacustrine basin, the Cangdong Sag later evolved into a downwarped to fault transition lacustrine basin due to regional tension (Pu et al., 2016; Han et al., 2021).

The Kongdian, Shahejie, and Dongying formations represent Paleogene deposits within the Cangdong Sag. Specifically, the Kongdian formation is subdivided into the Ek<sub>3</sub>, Ek<sub>2</sub>, and Ek<sub>1</sub> Members (Fig. 1). During the Paleogene, this region underwent five significant lake transgression events, resulting in the deposition of organic-rich source rocks. The Ek<sub>2</sub> Member, with a thickness ranging from 400 to 600 m (Pu et al., 2016), primarily consists of prodelta and semi-deep lacustrine sediments. Along the southern margin of the Cangdong Sag, wells G1, G2, and G3 were drilled within the Kongdian structural belt, revealing shales with promising oil potential (Zhao et al., 2019).

### 3. Samples and methods

A total of 63 shale samples from the  $Ek_2$  Member were collected from wells G1, G2, and G3 in the Cangdong Sag for thin section observation, X-ray diffraction (XRD), TOC content, extraction and fractionation, and multi-step programmed pyrolysis. Subsequently, 9 shale samples representing different lithofacies and TOC contents were chosen for pyrolysis-gas chromatography experiments (Table 1, Nos. 1–9). Additionally, twelve crude oil samples from  $Ek_2$  were obtained from 12 wells specifically for gas chromatography analysis (Fig. 1).

#### 3.1. Petrographic observation

The samples were mechanically polished into 30- $\mu$ m-thin sections perpendicular to the bedding to determine the mineral composition, sedimentary structure, and configuration of organic matter and minerals, using a Leica DM4P microscope under transmitted white light, reflected white light, and fluorescence (oil immersion objective) modes. Immersion oil (refractive index of 1.515) and oil immersion objectives were employed to increase the resolving power of the microscope.

#### 3.2. X-ray diffraction (XRD)

Powder samples were ground to approximately 200 mesh (approximately 0.075 mm) for XRD testing to determine their

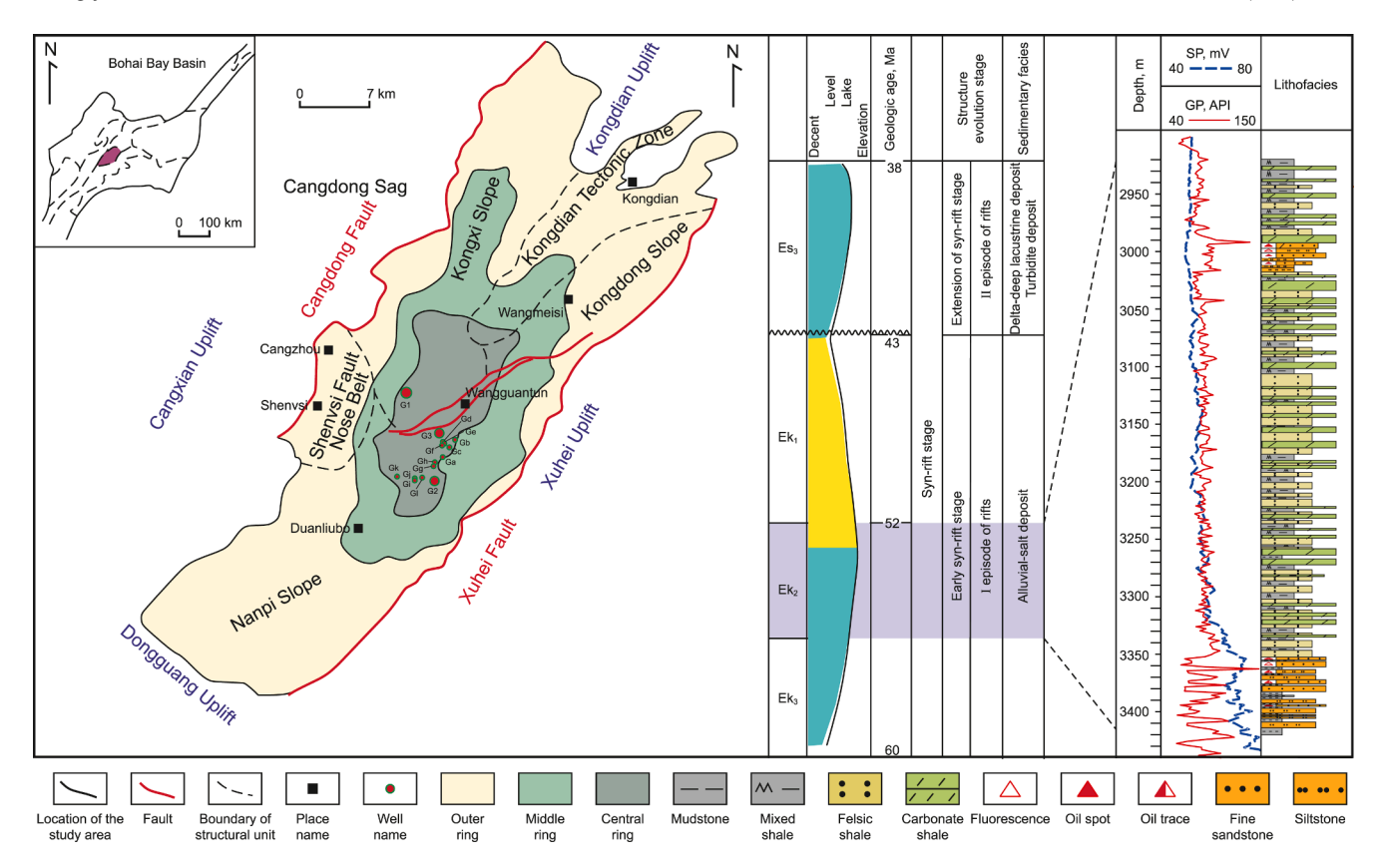


Fig. 1. Map, sedimentary facies and composite stratigraphic column of the second member of the Kongdian Formation, Cangdong Sag (modified from Pu et al., 2016; Deng et al., 2020; Li et al., 2020b).

mineralogy characterizations. To collect the XRD data a DX2700 X-ray diffractometer with CuK $\alpha$  radiation (40 kV, 40 mA) and Ni filtering was used. The tube voltage ranged from 15 to 60 kV and the tube current ranged from 5 to 60 mA with a maximum power of 3.3 kW. Samples were scanned from 2.5° to 30° with a step size of 0.02°.

# 3.3. Total organic carbon (TOC) analysis

Powder samples were ground to approximately 100 mesh (approximately 0.15 mm) for TOC content testing. Samples were treated with hydrochloric acid (HCl: water, 1:7, v/v) to remove carbonate minerals. Then samples were washed using distilled water to remove traces of HCl and oven-dried at 60  $\pm$  5 °C for 2 h. The TOC content was measured by a Leco CS-744 carbon and sulfur analyzer in an oxygenated combustion oven at a temperature of up to 1350 °C. A parallel sample was tested after every 20th sample and checked against the acceptable range.

# 3.4. Extraction and fractionation

Powder samples (approximately 100 mesh) were extracted with a mixture of dichloromethane with methanol (93:7 v/v) at  $60 \pm 5$  °C for 72 h using a Soxhlet apparatus. The extracted bitumen samples were treated with n-hexane to precipitate the asphaltene fractions. The resultant maltenes were further fractionated into a saturated hydrocarbon fraction, an aromatic hydrocarbon fraction, and a polar fraction by column chromatography using activated silica gel–alumina (3:2, v/v). Saturated and aromatic hydrocarbons were eluted with n-hexane

and a dichloromethane: petroleum ether (2:1, v/v) mixture, and polar fraction was eluted with dichloromethane.

# 3.5. Gas chromatography

The hydrocarbon compositions of 12 oil samples were characterized using gas chromatography. Less than 10 mg crude oil was dissolved in dichloromethane and tested by the Agilent GC 8890 gas chromatograph equipped with an HP-5MS capillary column (60 m  $\times$  0.25 mm  $\times$  0.25  $\mu m$  film thickness). The temperature was initially set at 50 °C with a holding time of 1 min and programmed to 120 °C at 20 °C/min, then to 325 °C at 3 °C/min with a final holding time of 25 min.

# 3.6. Pyrolysis-gas chromatography, and multi-step programmed pyrolysis

Powder samples were ground to approximately 100 mesh (approximately 0.15 mm) for pyrolysis testing. Pyrolysis-gas chromatography was performed using an American Weatherford single cold trap pyrolysis chromatograph to characterizing the compositions of thermal extracts, pyrolysis was performed using a Rock-Eval 6 instrument. Shale oil could be characterized at temperature below 450 °C (Jiang et al., 2016; Romero-Sarmiento, 2019). The programmed temperature system was divided into 10 sections: 0–200, 200–225, 225–250, 250–300, 300–325, 325–350, 350–375, 375–400, 400–425, and 425–450 °C. Every section has a heating rate of 25 °C/min and a final holding time of 3 min. Thermal extracts were collected using a liquid-nitrogen-cooled cryogenic trap (at –170 °C) and injected into an Agilent GC-6890N by ballistic heating (holding at 300 °C for 10 min) for gas

Petroleum Science 22 (2025) 3189–3206

**Table 1**TOC content and mineralogical compositions of shales for PY-GC (Nos. 1–9), and mineralogical compositions and bulk geochemical parameters of Ek<sub>2</sub> shale samples (Nos. 6–68).

Sample No.	Well ID	Depth, m	Siliciclastic minerals, wt%	Carbonate minerals, wt%	Clay minerals, wt%	TOC content, wt%		S <sub>1-2</sub> , mg HC/g rock	S <sub>2-1</sub> , mg HC/g rock	S <sub>2-2</sub> , mg HC/g rock	The corrected S <sub>1-1</sub> , mg HC/g rock	Saturates, wt%	Aromatics, wt%	Resins, wt%	Asphaltenes, wt%
1	G1	3280.40	34	34	26	2.60	1	1	1	1	1	44	12	23	21
2	G2	3892.56	60	30	10	3.74	j	1	1	Ï		42	11	29	26
3	G3	4099.93	58	30	12	2.96	, I	1	1	Ï		50	13	17	14
4	G3	4117.26	38	49	13	2.70	,	1	1	,	,	51	16	19	10
5	G3	4125.84	46	39	15	3.15	1	1	1	1	1	44	12	18	20
6	G1	3043.53	26	4	17	1.32	0.72	1.70	1.15	8.19	1	38	11	25	27
7	G1	3148.60	17	50	17	0.93	1.17	5.33	1.4	2.94	1	24	7	16	53
8	G2	3824.49	21	53	19	0.79	0.21	0.11	0.01	0.25	1	34	8	19	39
9	G2	3860.35	19	69	12	2.36	1.50	0.97	0.14	0.52	1	48	10	25	17
10	G1	2970.47	20	37	25	0.55	0.09	0.27	0.20	1.23	1	22	8	21	48
11	G1	2972.21	34	23	27	6.89	0.42	1.31	3.24	30.04	1	21	11	24	45
12	G1	2972.45	12	43	27	2.42	0.64	1.87	3.37	23.07	1	21	11	24	45
13	G1	2972.91	15	28	34	2.95	0.38	1.41	2.53	16.57	/	31	15	34	19
14	G1	2984.85	18	59	8	1.00	0.65	1.50	1.21	8.31	/	31	15	34	19
15	G1	2985.17	14	65	5	2.35	1.53	6.02	4.46	15.88	1	29	8	29	33
16	G1	3040.33	21	11	27	3.52	0.57	1.06	1.57	14.62	1	33	11	30	26
17	G1	3118.10	43	10	26	3.07	0.60	1.48	2.00	19.17	1	25	15	33	27
18	G1	3165.20	13	45	28	0.68	0.13	0.22	0.10	1.09	1	26	8	26	40
19	G1	3274.97	39	6	50	0.99	0.11	0.76	1.17	9.63	/	35	11	32	22
20	G1	3283.72	18	3	41	3.37	0.48	1.19	1.84	18.03	0.73	25	9	29	37
21	G2	3820.33	49	17	18	1.10	0.36	0.18	0.03	0.80	0.73	35	9	18	38
22 23	G2	3820.63 3824.52	59	36	4	1.91	2.85	4.06	1.17	4.62	5.79 0.85	52	11	14 23	22
	G2		41	35	11	0.80	0.42	0.32	0.24	0.45		40	13		24
24 25	G2 G2	3829.78 3834.84	32 41	6 8	36 23	0.89 0.57	0.05 0.03	0.11 0.03	0.04 0.01	0.25 0.05	0.10 0.06	26 43	11 11	19 21	44 23
26	G2 G2	3836.39	25	66	9	2.71	1.89		2.15	8.46	3.84	45 36	15	27	23
26	G2 G2	3845.03	25 76	17	7	1.93	2.20	4.28 3.84	1.53	6.47	3.84 4.47	36 35	12	27	31
28	G2 G2	3853.64	65	27	8	3.36	2.27	3.16	1.75	12.59	4.61	39	12	26	23
29	G2 G2	3854.97	26	64	10	1.89	0.97	1.29	0.28	0.90	1.97	58	13	23	6
30	G2	3857.45	60	35	5	2.14	2.63	3.30	1.17	7.00	5.34	60	11	16	13
31	G2	3858.74	59	35	6	1.46	1.58	2.03	0.71	4.32	3.21	44	12	23	21
32	G2	3862.93	20	37	31	0.45	0.16	0.40	0.03	0.21	0.32	46	7	24	22
33	G2	3865.43	67	28	5	2.49	2.61	3.54	1.54	9.67	5.30	47	12	20	21
34	G2	3869.10	71	15	9	1.67	2.75	4.47	2.16	12.64	5.58	44	10	20	26
35	G2	3870.29	32	54	14	1.91	1.75	2.34	1.11	6.61	3.55	47	14	26	13
36	G2	3871.70	47	44	5	2.00	2.32	3.38	1.82	12.52	4.71	55	12	22	10
37	G2	3872.88	27	50	23	2.40	2.71	4.09	1.88	7.68	5.50	50	16	24	10
38	G2	3878.62	61	27	11	2.93	1.75	3.69	2.04	14.83	3.55	66	10	16	8
39	G2	3885.56	69	26	5	2.79	1.73	2.58	0.89	5.06	3.51	52	12	20	16
40	G2	3888.38	46	12	42	1.36	3.54	3.70	0.55	1.04	7.19	53	8	25	14
41	G2	3888.72	32	32	31	3.06	4.36	5.90	1.55	3.36	8.85	49	12	21	17
42	G2	3889.51	39	44	17	3.30	3.11	6.23	2.67	11.72	6.31	43	11	25	21
43	G2	3894.93	26	37	37	2.52	2.62	5.87	2.73	8.14	5.32	48	15	24	13
44	G2	3901.43	65	17	17	4.68	2.69	4.11	2.60	38.99	5.46	44	15	27	13
45	G3	4076.32	27	40	23	0.78	0.20	0.50	0.27	0.93	0.41	37	12	19	31
46	G3	4077.89	13	54	21	0.48	0.08	0.20	0.09	0.37	0.16	47	12	19	22
47	G3	4078.81	40	30	17	0.97	0.68	1.12	0.49	1.54	1.38	57	12	18	13
48	G3	4079.92	32	43	22	1.62	1.03	2.12	1.14	5.08	2.09	52	16	14	18
49	G3	4081.33	16	57	20	0.78	2.17	4.08	2.29	14.88	4.41	46	14	16	23
50	G3	4081.42	43	33	13	2.07	1.64	3.33	1.50	7.91	3.33	56	17	15	12
51	G3	4084.46	41	37	15	1.77	4.92	6.20	2.90	7.03	9.99	32	10	17	41
52	G3	4085.95	46	35	19	2.93	3.64	6.09	2.25	9.71	7.39	55	16	18	11
53	G3	4087.15	34	49	13	0.95	2.79	6.34	1.64	3.98	5.66	60	12	17	12
	G3	4087.52	82	13	4	2.15	5.58	9.48	2.32	5.73	11.33	40	15	23	22

6	14	13	10	∞	17	21	17	11	29	22	16	28	56
17	17	16	25	29	19	16	23	26	16	25	29	19	15
12	11	15	15	16	15	13	14	14	13	10	13	13	10
61	28	57	20	47	20	20	46	20	42	42	42	40	48
4.83	1.14	0.83	3.25	4.04	2.56	3.92	5.22	2.48	3.09	3.59	2.78	3.19	3.25
4.33	0.90	0.57	25.06	26.72	9.40	6.75	17.56	5.53	22.18	12.19	8.28	9.73	7.51
1.16	0.23	0.10	1.89	2.80	0.83	1.64	2.55	1.19	1.71	2.28	1.00	1.33	0.95
3.34	0.65	0.37	2.16	4.12	1.62	3.47	4.11	2.13	2.14	3.87	1.57	1.9	2.00
2.38	0.56	0.41	1.60	1.99	1.26	1.93	2.57	1.22	1.52	1.77	1.37	1.57	1.60
1.73	0.64	0.50	3.95	3.71	1.59	1.91	3.84	1.57	3.71	2.99	2.81	2.68	6.53
24	11	29	6	4	13	7	5	5	9	4	3	4	2
36	41	31	8	16	29	42	24	53	22	35	39	35	47
38	33	29	82	80	51	48	89	42	69	29	28	29	48
4087.94	4091.45	4096.32	4103.39	4106.88	4109.77	4119.38	4127.49	4131.89	4132.36	4137.78	4140.33	4141.61	4142.81
63	63	C3	C3	63	63	63	63	63	C3	C3	63	63	63
55	26	22	28	29	09	61	62	63	64	65	99	29	89

chromatographic analysis (HP-Ultra, 50 m  $\times$  32 mm [164 ft  $\times$  1.26 in] inner diameter, dimethylpolysiloxane-coated column with 0.52  $\mu$ m [2.0  $\times$  10<sup>-5</sup> in] film thickness).

Multi-step programmed pyrolysis was performed using a Rock-Eval 6 instrument to characterizing the content of shale oil in different occurrence states.  $S_{1-1}$  (movable hydrocarbons) was measured at 225 °C (3 min),  $S_{1-2}$  (medium-to-high molecular weight hydrocarbons) was measured by a programmed temperature system from 225 °C (0 min) to 350 °C (3 min) at 25 °C/min,  $S_{2-1}$  (adsorbed hydrocarbons) was measured by a programmed temperature system from 350 °C (0 min) to 400 °C (3 min) at 25 °C/min, and  $S_{2-2}$  (kerogen-cracking hydrocarbons) was measured by a programmed temperature system from 400 °C (0 min) to 600 (3 min) at 25 °C/min (Fig. 2).

#### 4. Results

#### 4.1. Mineral composition and TOC content

The Ek<sub>2</sub> shale samples primarily consist of felsic minerals (quartz and feldspar), carbonate minerals (calcite and dolomite), and clay minerals. Felsic minerals are the most abundant, averaging 41 wt%, while carbonate minerals and clay minerals constitute 34 wt% and 17 wt%, respectively (Table 1, Nos. 6-68). The felsic minerals and clay minerals in the study area are mainly originated from terrigenous clasts (Zhao et al., 2023). To elucidate the influence of mineral composition on shale oil occurrence state, the shale samples were categorized as felsic, carbonate, and argillaceous when the corresponding component exceeded 50 wt%, and as mixed shale when no single component constituted more than 50 wt% of the composition. In the study area, the Ek2 Member primarily consists of felsic, carbonate, and mixed shales (Fig. 3). The TOC content of felsic shales is relatively high, with an average of 2.48 wt%, while the average TOC content of mixed and carbonate shales is 2.25 wt% and 1.49 wt%, respectively.

#### 4.2. Sedimentary structure and maceral characteristics

The Ek2 shale can be categorized into three types based on sedimentary structure: laminated shale (single bed thickness <1 mm), bedded shale (1 mm < single bed thickness <1 cm), and massive mudstone (lacking bedding) (Fig. 4). In laminated shale, the laminae are predominantly flat, though irregularly shaped and interrupted laminae are also observed (Fig. 4(b) and (c)). The laminae are categorized into four types based on their mineral compositions: felsic, carbonate, argillaceous, and mixed laminae (Fig. 4(c)). The macerals identified include alginate, liptinite, vitrinite, inertinite, and secondary components (Fig. 5). Liptinite and secondary components are the predominant constituents, comprising 89% of the total maceral content, while the vitrinite and inertinite together account for 11% (Fig. 5(i)). Telalginite and lamalginite, which are prone to hydrocarbon generation, tended to concentrate in argillaceous laminae (Fig. 5(a) and (b)). The interconnected pores within felsic laminae are well-developed and contain secondary components, such as oil exudates (Fig. 5(a) and (b)). Carbonate laminae are primarily composed of micritic and crystalline carbonate minerals, which exhibited tightly packed internal structures with minimal maceral development (Fig. 5(e) and (f)). In massive mudstones, the internal macerals are more mixed compared to those in laminated shales (Fig. 5(c)).

#### 4.3. Extractable organic matter

The extractable organic matter content of 63 samples ranges from 0.09 to 2.95 wt%, with an average of 0.86 wt%. Samples from

well G1 have a relatively low content, ranging from 0.09 to 0.63 wt%, with an average of 0.24 wt%. In contrast, samples from well G2 range from 0.13 to 2.38 wt%, with an average of 1.06 wt%, while those from well G3 range from 0.16 to 2.95 wt%, with an average of 0.99 wt%.

The extractable organic matter content in different lithofacies is ranked as follows: felsic shale (1.13 wt%) > calcareous dolomitic shale (0.73 wt%) > mixed shale (0.67 wt%). The proportions of saturates, aromatics, resins, and asphaltenes are similar in wells G2 and G3, with saturates being the predominant component, ranging from 26 to 70 wt%, and average proportions of 46 and 49 wt%, respectively. In contrast, samples from well G1 primarily contain higher proportions of asphaltenes, ranging from 19 to 53 wt%, with an average of 34 wt% (Fig. 6; Table 1, Nos. 6–68).

# 4.4. Shale pyrolysis characteristics and crude oil n-alkane distribution

Pyrolysis-gas chromatography experiment was conducted over 10 temperature intervals ranging from 0 to 450 °C with a heating rate of 25 °C/min (Fig. 7). The PY-GC results of samples from wells G2 and G3 exhibit similar characteristics (Fig. 7). Although a small number of n-alkenes are observed at 300–350 °C, the pyrolysis products are mainly n-alkanes below 350 °C (Fig. 7(a)–(f)). Above 350 °C, the pyrolysis products are predominantly light hydrocarbons and unsaturated organic compounds (Fig. 7(g) and (h)). Methane is observed at temperatures above 400 °C (Fig. 7(i) and (j)). The results of samples from well G1 are generally similar to those from wells G2 and G3, but alkenes begin to generated between 325 °C and 350 °C (Fig. S1). Gas chromatography results indicate that the 12 crude oil samples exhibit similar characteristics, with n-C22 as the main peak carbon and small content of n-C30 hydrocarbon compounds (Fig. 7(k) and (l); Fig. S2).

# 4.5. Multi-step programmed pyrolysis

The results of the multi-step programmed pyrolysis experiment for 13 samples from well G1 reveal average values of 0.58 mg HC/g rock for S<sub>1-1</sub>, 1.86 mg HC/g rock for S<sub>1-2</sub>, 1.86 mg HC/g rock for S<sub>2-1</sub>, and 12.98 mg HC/g rock for S<sub>2-2</sub>. For 26 samples from well G2, the average values are 1.89 mg HC/g rock for S<sub>1-1</sub>, 2.85 mg HC/g rock for S<sub>1-2</sub>, 1.18 mg HC/g rock for S<sub>2-1</sub>, and 6.89 mg HC/g rock for S<sub>2-2</sub>. For 24 samples from well G3, the average values are 1.85 mg HC/g rock for S<sub>1-1</sub>, 3.04 mg HC/g rock for S<sub>1-2</sub>, 1.44 mg HC/g rock for S<sub>2-1</sub>, and 8.91 mg HC/g rock for S<sub>2-2</sub> (Fig. 8; Table 1, Nos. 6–68).

The pyrolysis hydrocarbon content of felsic shales averages 2.03 mg HC/g rock for  $S_{1-1}$ , 3.14 mg HC/g rock for  $S_{1-2}$ , 1.54 mg HC/g rock for  $S_{2-1}$ , 12.19 mg HC/g rock for  $S_{2-2}$ . In comparison, mixed shales exhibit slightly lower pyrolysis hydrocarbon content:

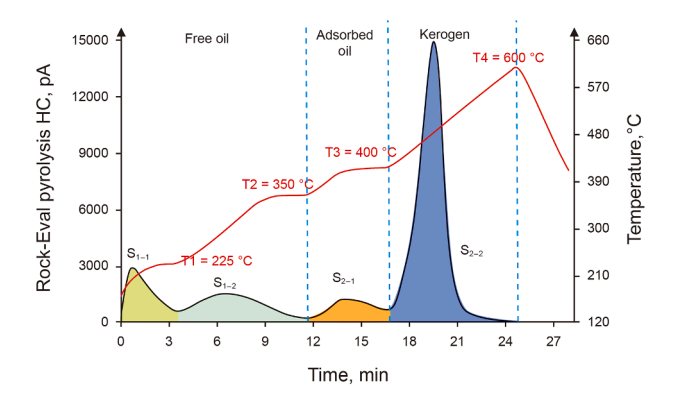


**Fig. 2.** The Rock-Eval pyrogram generated by Ek<sub>2</sub> shales.

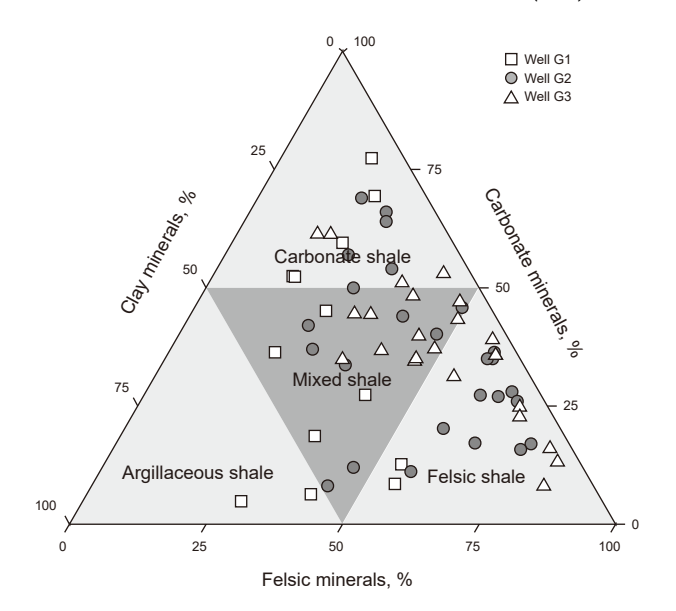


Fig. 3. The lithological classification of the  ${\rm Ek}_2$  shales based on mineralogical compositions.

1.85 mg HC/g rock for  $S_{1-1}$ , 2.89 mg HC/g rock for  $S_{1-2}$ , 1.16 mg HC/g rock for  $S_{2-1}$ , 4.73 mg HC/g rock for  $S_{2-2}$ . Carbonate shales show the lowest pyrolysis hydrocarbon content: 1.69 mg HC/g rock for S<sub>1-1</sub>. 2.85 mg HC/g rock for  $S_{1-2}$  1.19 mg HC/g rock for  $S_{2-1}$  5.42 mg HC/g rock for S<sub>2-2</sub>. (Fig. 9(a)). Overall, laminated shales exhibit the highest pyrolysis hydrocarbon content, with average value of  $2.05 \text{ mg HC/g rock for S}_{1-1}$ ,  $3.28 \text{ mg HC/g rock for S}_{1-2}$ , 1.55 mg HC/grock for S<sub>2-1</sub>, and 11.16 mg HC/g rock for S<sub>2-2</sub>. Conversely, massive mudstones exhibit the lowest pyrolysis hydrocarbon content, with averages of 1.51 mg HC/g rock for  $S_{1-1}$ , 2.33 mg HC/g rock for  $S_{1-2}$ , 0.99 mg HC/g rock for S<sub>2-1</sub>, and 4.67 mg HC/g rock for S<sub>2-2</sub> (Fig. 9 (b)). Pyrolysis-gas chromatography results indicate that the components of movable oil  $(S_{1-1})$  and immovable oil  $(S_{1-2})$  within free oil are similar, suggesting the potential of mutual transformation during exploitation, with no clear boundary existing between them. Therefore, the combined free oil content  $(S_{1-1} + S_{1-2})$  will be consistently referenced in subsequent discussions.

#### 5. Discussion

# 5.1. Quantitative characterization of shale oil in different occurrence states

#### 5.1.1. Scheme of multi-step programmed pyrolysis

The pyrolysis properties of shale are primarily influenced by oil content, kerogen type, and thermal maturity. Shales from wells G2 and G3 with varying TOC content and lithofacies exhibited similar chromatographic characteristics within the same temperature interval. This indicates that pyrolysis characteristics are predominantly controlled by organic properties, rather than mineral composition or other inorganic characteristics. Consequently, shale oil in different occurrence states in different lithofacies from the Ek2 can be effectively characterized using a unified multi-step programmed pyrolysis scheme. The only noted difference in chromatographic characteristics between the thermal extracts below 350 °C and crude oil was the proportion of each component (Fig. 7), indicating that the components released during these temperature intervals consist of movable oil and heavy free oil. Numerous light hydrocarbons and unsaturated organic compounds are generated during the pyrolysis of crude oil and asphaltene (Behar et al., 1992,

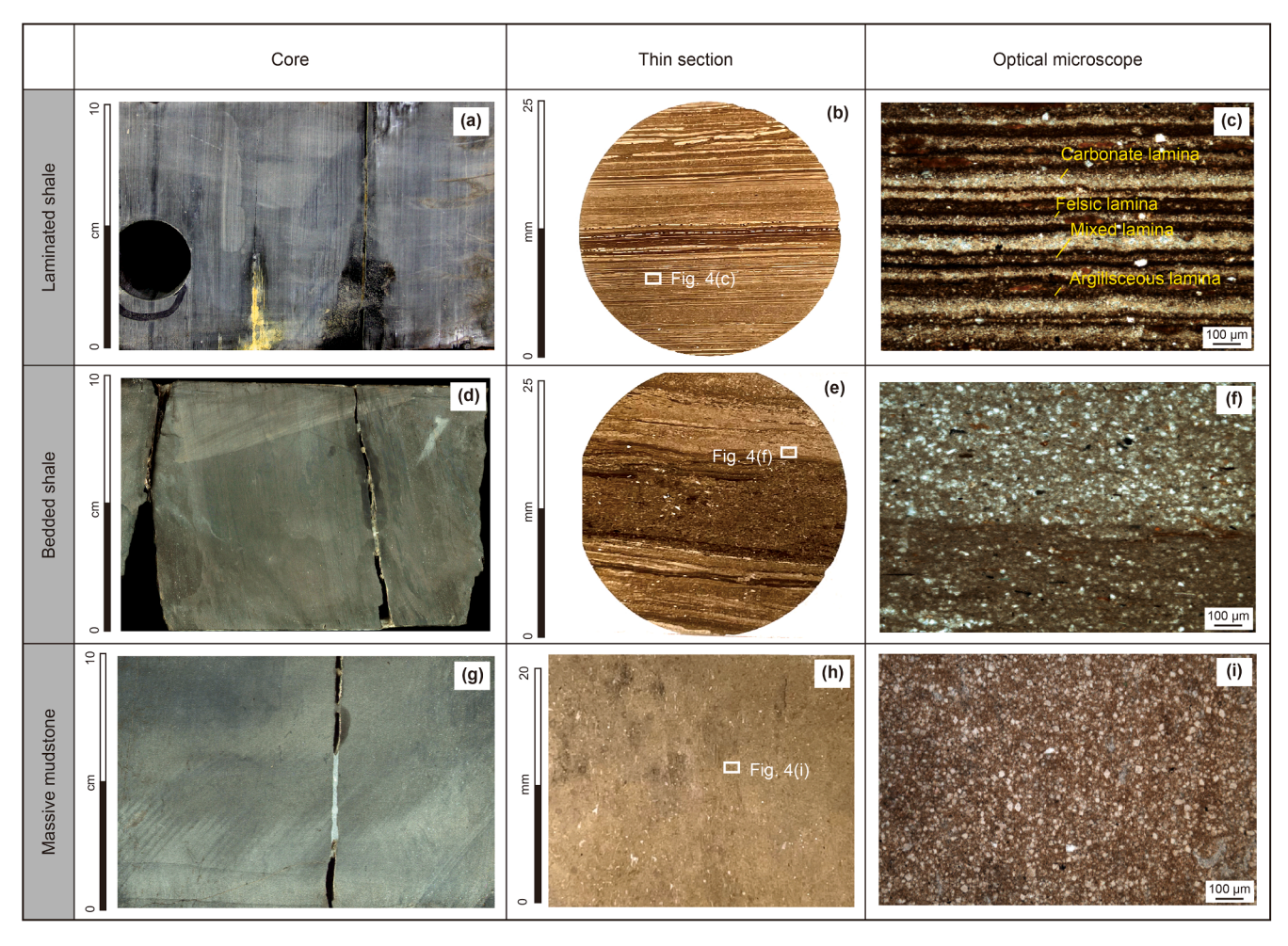


**Fig. 4.** Core images and thin section photomicrographs of shales with different sedimentary structures. (a) Core image of laminated shale, well G2, 3878.62 m. (b) Thin section photomicrograph of laminated shale, plane-polarized light, well G2, 3878.62 m. (c) Zoom view of laminated shale, plane-polarized light, well G2, 3878.62 m. (d) Core image of bedded shale, well G1, 3075.26 m. (e) Thin section photomicrograph of bedded shale, plane-polarized light, well G1, 3075.26 m. (g) Core image of massive mudstone, well G3, 4099.93 m. (h) Thin section photomicrograph of massive mudstone, plane-polarized light, well G3, 4099.93 m. (i) Zoom view of massive mudstone, plane-polarized light, well G3, 4099.93 m.

1997; Gentzis et al., 2021), consistent with the chromatographic characteristics observed in thermal extracts above 350 °C in this study (Fig. 7(g)-(i)). Methane occurs at pyrolysis temperatures above 400 °C (Fig. 7(i) and (j)), with a rapid increase in methane content highlighting a key distinction between kerogen-cracking gas (direct cracking to gas) and crude oil-cracking gas (Behar et al., 1992). PY-GC results of samples from well G1  $(0.7\% < R_0 < 0.9\%)$  show that alkenes begin to generate between 325 °C and 350 °C (Fig. S1), suggesting slightly lower temperature threshold for the release of adsorbed oil. However, the instrumental temperature uncertainty ( $\pm 10$  °C) limits further differentiation of the pyrolysis behavior of samples from well G1. To ensure the general applicability of the pyrolysis method for Ek<sub>2</sub> shale, a unified multi-step programmed pyrolysis scheme has been established. Thermal extracts below 350  $^{\circ}$  C (S<sub>1-1</sub> + S<sub>1-2</sub>), between 350 and 400  $^{\circ}$  C (S2-1), above 400  $^{\circ}\text{C}$  (S2-2) correspond to free oil, adsorbed oil, and hydrocarbons generated from kerogen, respectively.

Significantly, some high molecular weight components of free oil are challenging to produce due to their limited mobility, presenting a potential exploitation resource as technology advances. Jarvie (2012) emphasized that recoverable resources are available only when  $S_1\times 100/TOC > 100$  mg HC/g TOC, indicating that some free oil cannot be exploited due to the strong

adsorption capacity of organic matter. Previous studies have shown that thermal extracts released at 0-200 °C primarily consist of low-to-medium molecular weight hydrocarbons below n-C<sub>20</sub> or n-C<sub>24</sub> (Romero-Sarmiento et al., 2016), corresponding to movable oil (Jiang et al., 2016). However, although the content of the high molecular weight components (above  $n-C_{25}$ ) in mobile oil is relatively low, these can constitute up to 24% of crude oil (Fig. 7(k) and (1)), necessitating higher temperatures for full characterization. The pyrolysis-gas chromatographic characteristics of shale samples below 225 °C are consistent with those of crude oil (Fig. 7(b)), indicating that the movable oil content can be effectively characterized by Rock-Eval pyrolysis at temperature at 225 °C. A quantitative characterization method has been established for shale oil in different occurrence states from medium-maturity shale in the Ek2, Cangdong Sag. This method optimizes temperature and residence time settings for each pyrolysis stage (Fig. 10(a)), and effectively addresses the "shoulder" observed in the pyrolysis curve, which results from incomplete hvdrocarbon release at certain temperatures (Fig. 10(b)-(f)) (Ma et al., 2023). Compared to the method proposed by Jiang et al. (2016), this approach provides more accurate characterization of shale oil in different occurrence states and is better suited for the Ek<sub>2</sub> shale.

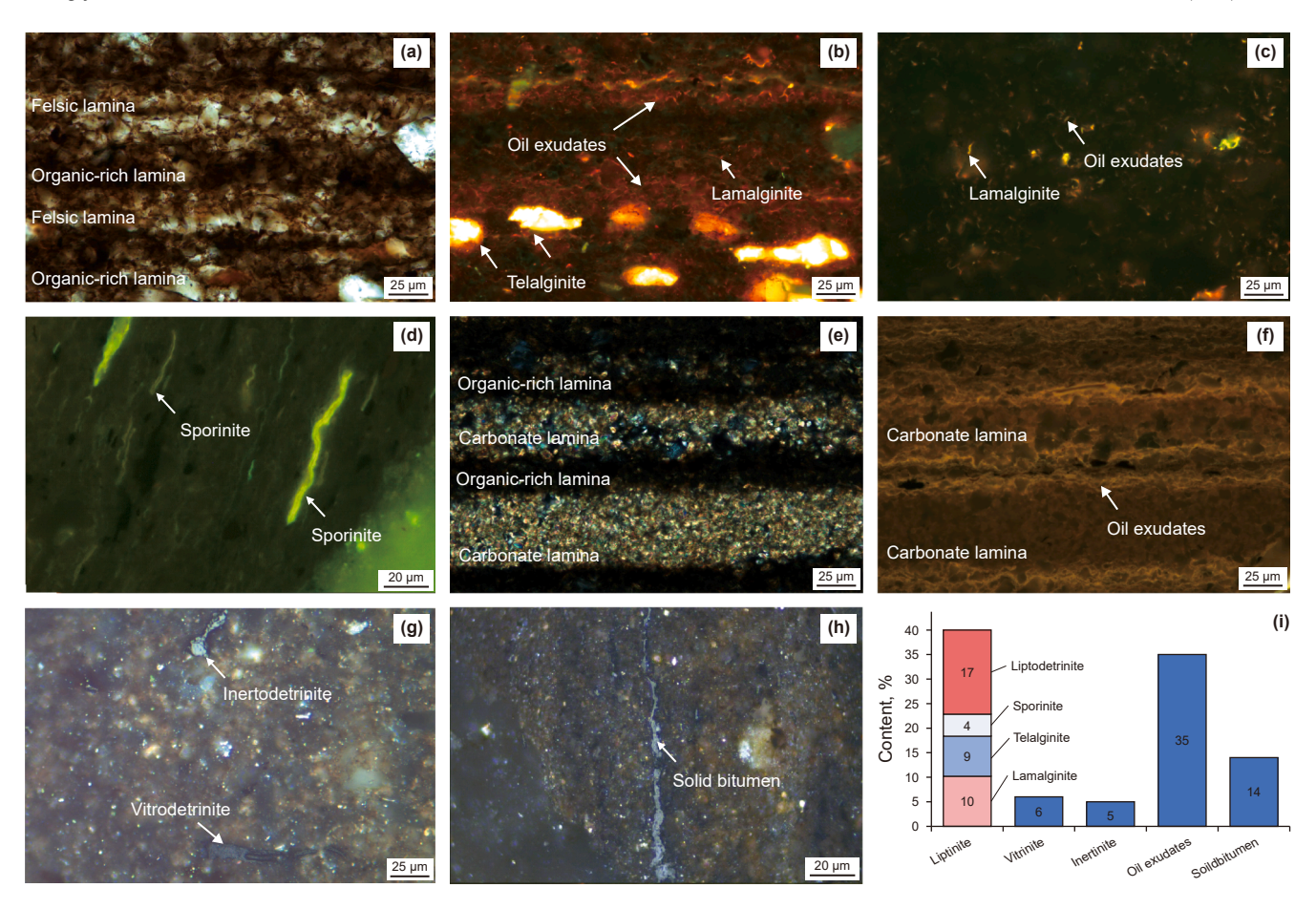


**Fig. 5.** Photomicrographs of Ek<sub>2</sub> shale. (a) Photomicrograph of interbedding of felsic and organic-rich laminae in laminated shale, plane-polarized light in oil immersion, well G2, 3876.48 m. (b) Photomicrograph of distribution of macerals in laminated shale, oil exudates concentrate in felsic laminae and alginates concentrate in organic-rich laminae, fluorescent light (blue-light excitation) in oil immersion, well G2, 3876.48 m. (c) Photomicrograph of distribution of macerals in massive mudstone, there is no regularity in distribution of oil exudates and alginates, fluorescent light (blue-light excitation) in oil immersion, well G3, 4084.46 m. (d) Photomicrograph of sporinites, fluorescent light (blue-light excitation) in oil immersion, well G1, 3281.19 m. (e) Photomicrograph of interbedding of carbonate and organic-rich laminae in laminated shale, cross-polarized light in oil immersion, well G1, 3104.70 m. (f) Photomicrograph of distribution of macerals in laminated shale, there is little oil exudates concentrate in carbonate laminae, fluorescent light (blue-light excitation) in oil immersion, well G1, 3104.70 m. (g) Photomicrograph of inertodetrinite and vitrodetrinite, reflected white light in oil immersion, well G2, 3866.05 m. (h) Photomicrograph of solid bitumen, reflected white light in oil immersion, well G2, 3878.80 m. (i) The content of different kinds of macerals.

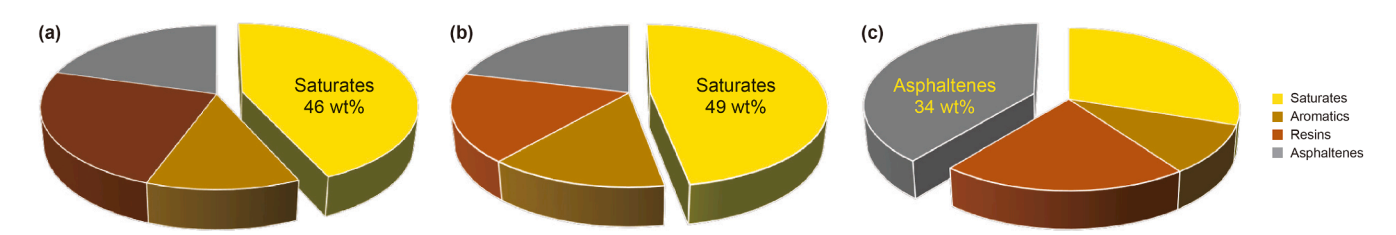


Fig. 6. Average chemical compositions of extractable organic matter in shales from well G2 (a), well G3 (b), and well G1 (c).

5.1.2. Compensation correction of light hydrocarbon components

Light hydrocarbons are often lost during sample preservation and preparation due to their high volatility (Cooles et al., 1986; Michael et al., 2013). In this study, freshly extracted crude oil with minimal light hydrocarbon loss, collected from development wells near G2 and G3 in Ek<sub>2</sub>, was used as the standard of light hydrocarbon components. Since GC data for fresh crude oil were available from only 4 production wells (data provided by the Exploration and Development Research Institute, Dagang Oilfield Company, PetroChina), light hydrocarbon correction was based on comparing their GC results with the PY-GC data of shale samples from wells G2 and G3 (Table 1, Nos. 2–5, 8–9).

Considering the impact of production time on crude oil components, 4 fresh crude oil samples from different production periods were selected, and the average values of gas chromatography–derived n-alkanes ratios were utilized to calculate the light hydrocarbons correction coefficient (Fig. 11). To minimize the lost light hydrocarbons content, the time interval between sampling and analysis was maintained within 2 h. According to the hydrocarbon generation kinetics correction methods, the lost hydrocarbon components are typically n-C $_{13}$  (Lu, 1996; Li et al., 2016). However, comparisons between gas chromatography of all fresh crude oil and pyrolysis-gas chromatography of shale samples reveal that n-C $_{17}$  components are

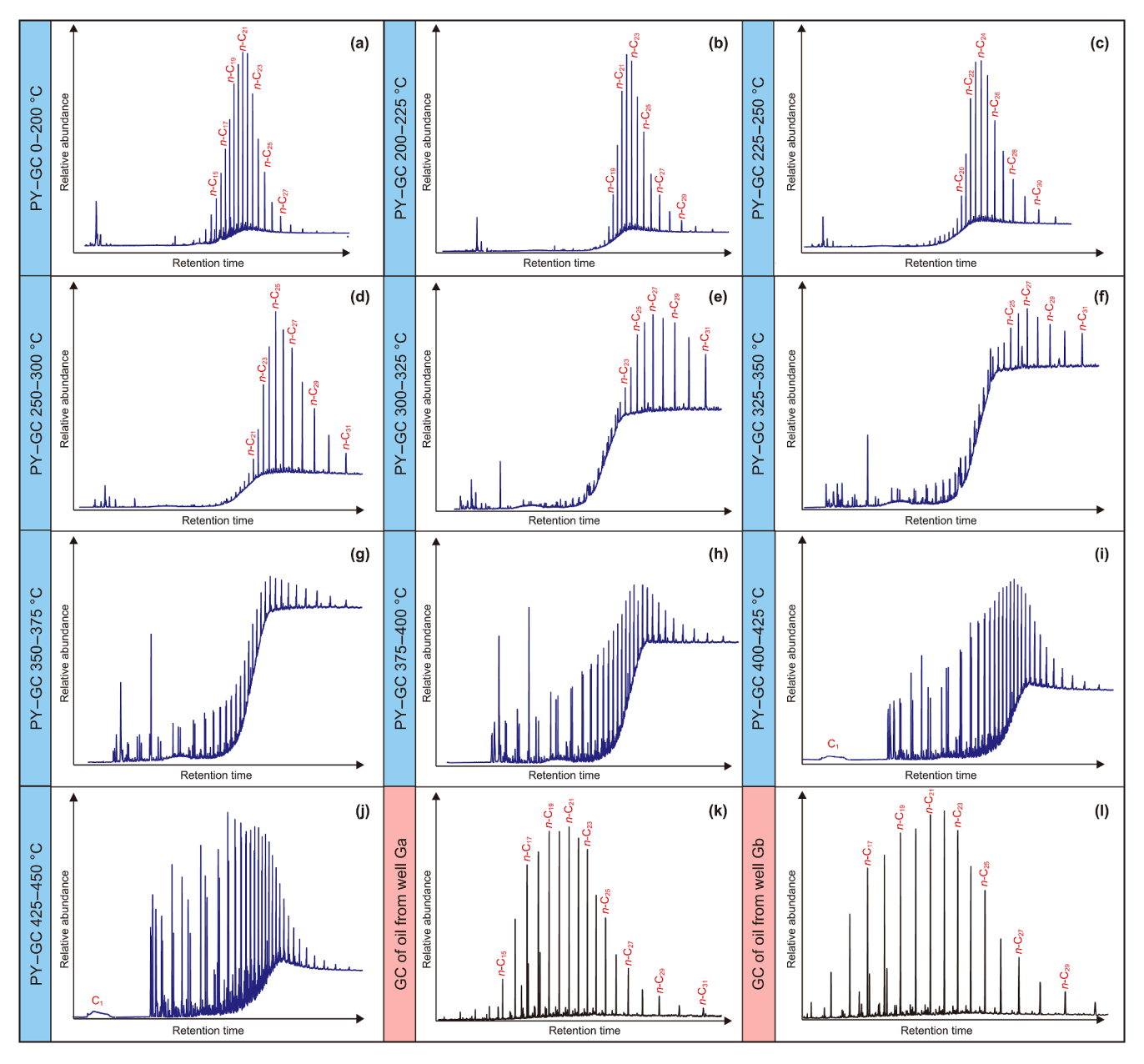


Fig. 7. Results of pyrolysis-gas chromatogram for the shale from well G3 and gas chromatogram for the crude oil from wells Ga and Gb. Compositions of thermal extracts at 0–200 °C (a), 200–225 °C (b), 225–250 °C (c), 250–300 °C (d), 300–325 °C (e), 325–350 °C (f), 350–375 °C (g), 375–400 °C (h), 400–425 °C (i), and 425–450 °C (j). Compositions of crude oil from wells Ga (k) and Gb (l).

lost in our shale samples (Fig. 11). Therefore, this study corrects for the n- $C_6$  to n- $C_{17}$  components in this study. After comparing crude oil gas chromatograms and pyrolysis-gas chromatograms of shale samples below 225 °C, the light-to-heavy component ratio (R) was calculated using the average values (AVG) of n-alkane components from 4 crude oil samples collected from development wells as the standard:

$$R = \sum AVG(n-C_{x,oil}) / \sum AVG(n-C_{y,oil}),$$

$$x = 6, 7, ..., 17; y = 18, 19, ..., 30$$
(1)

The theoretical total light hydrocarbon content  $(S_T)$  is calculated as:

$$S_T = R \times S_{1-1} \times (n - C_{18^+ \text{rock}} / n - C_{6^+ \text{rock}})$$
 (2)

the  $n-C_{18}^{+}$  and  $n-C_{6}^{+}$  are calculated from the PY-GC

(below 225 °C) result. The lost light hydrocarbons content ( $S_L$ ) is calculated by subtracting the residual n- $C_{17}^-$  in the sample:

$$S_L = S_T - S_{1-1} \times (n - C_{17^- \text{rock}} / n - C_{6^+ \text{rock}})$$
 (3)

the  $n\text{-C}_{17}^-$  rock and  $n\text{-C}_6^+$  rock are calculated from the PY-GC (below 225 °C) result.

The average light-to-heavy component ratio (R) of the crude oil samples is 1.24. The average of  $n-C_{18}^+_{rock}/n-C_{6}^+_{rock}$  of 6 rock samples from wells G2 and G3 is 0.91. Consequently, the lost light hydrocarbons content ( $S_L$ ) is 1.03  $\times$   $S_{1-1}$ , and the light hydrocarbon correction coefficient (K) for  $S_{1-1}$  is determined using the formula:

$$K = (S_{1-1} + S_L)/S_{1-1} (4)$$

The calculated value of *K* is 2.03, which is consistent with previous studies (Cooles et al., 1986; Michael et al., 2013; Dou et al., 2024). Although a small content of light hydrocarbons lost during

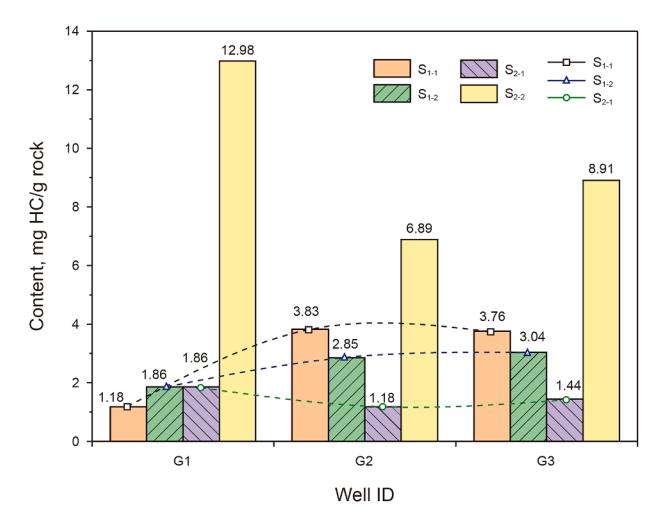


Fig. 8. Average thermal extracts content of shales from three wells.

crude oil extraction and experimentation, complete retention of these components during commercial exploitation and transportation remains challenging. Consequently, the recovery results presented in this study realistically reflect the actual available resources to the greatest extent. The average lost light hydrocarbons content is 2.05 mg HC/g rock in this study (Table 1, Nos. 21–68), and the average value of  $S_1$  in  $Ek_2$  shale is 2.37 mg HC/grock (without correction of light hydrocarbons) (Zhao et al., 2019). Accordingly, the correction coefficient for conventional pyrolysis S<sub>1</sub> is approximately 1.87. This value closely aligns with the recovery coefficient (1.89) from pressure-holding closed coring samples in Ek<sub>2</sub> (Dou et al., 2024). It is worth noting that the adsorption capacity of aliphatic chains is strong (Liang et al., 2021), shale samples with high liptinite content and low thermal maturity may experience minimal hydrocarbon loss. During thermal maturity, changes in internal functional groups and microscopic structure occur due to hydrocarbon generation and cracking, affecting the coefficient of compensation correction for light hydrocarbon components. However, these changes are inconsistent and cannot be accurately and quantitatively characterized (Yang et al., 2017). Li et al. (2016) also suggested that the hydrocarbon recovery coefficient is largely influenced by the maturity of organic matter. Consequently, the light hydrocarbon recovery method proposed in this study offers new insights for future research on light hydrocarbon recovery. It is important to note that the obtained values are specific to shale samples at a particular maturity in the Ek<sub>2</sub>,

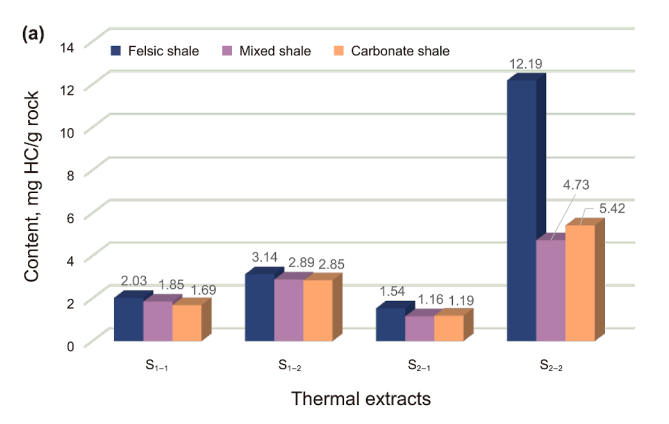
Cangdong Sag. The compensation standard for light hydrocarbon components cannot be generalized and must be analyzed at different thermal maturity levels.

### 5.2. Influencing factors of shale oil occurrence state

# 5.2.1. The effect of organic matter content and its thermal maturity

The maturity of organic matter is a critical factor influencing shale oil content and its occurrence state. Lewan (1985) reported that the content of kerogen decreases while the content of expelled oil increases with rising maturity within the oil window, as demonstrated in rock thermal simulation for hydrocarbon generation on Phosphoria Retort shale. These findings are consistent with observations from Woodford and Barnett shales (Jarvie et al., 2007). In this study, variations in the maturity of shale samples from the three wells were noted. The thermal maturity of shale samples from well G1 is relatively low  $(0.7\% < R_0 < 0.9\%)$ . while samples from wells G2 and G3 exhibit similar and high maturity levels (0.9%  $< R_0 < 1.0$ %) (Zhao et al., 2019). Correspondingly, the free oil content  $(S_{1-1} + S_{1-2})$  is relatively low in well G1, consistent with the low content of saturated hydrocarbons (Fig. 6), indicating that the proportion of mobile components is small. In contrast, the further cracking of kerogen and retained oil in wells G2 and G3 results in a different shale oil occurrence state, characterized by high free oil content  $(S_{1-1} + S_{1-2})$ , low adsorbed oil content (S2-1), and low kerogen cracked hydrocarbon content (S<sub>2-2</sub>) (Fig. 8), along with reduced asphaltene fractions (Fig. 6).

Kerogen consists of "dead carbon", which lacks hydrocarbongenerating capacity, and hydrocarbon-generating organic matter (Cooles et al., 1986; Merrill, 1991), only the latter of which can be represented by pyrolysis S<sub>2-2</sub>. Although the total pyrolysis hydrocarbon content  $(S_{1-1} + S_{1-2} + S_{2-1} + S_{2-2})$  shows a significant positive correlation with TOC content, there are some points have no regularity (Fig. 12(a)). Adsorbed oil is primarily composed of high molecular weight organic compounds (Cady and Seelig, 1952), and consistently bound to aliphatic organic matter due to their similar molecular structure (McIver, 1967; Vandenbroucke and Largeau, 2007; Liang et al., 2021). Due to the high degree of aromatization, the oil adsorbed by dead carbon is significantly lower than that adsorbed by hydrocarbon-generating macerals. To provide a practical assessment of kerogen's adsorption capacity, the  $S_{2-2}$  value, rather than the TOC content, is used to represent kerogen content in this study. Adsorbed oil content exhibits a stronger positive correlation with  $S_{2-2}$  ( $R^2 = 0.65$  for samples from wells G2 and G3;  $R^2 = 0.63$  for samples from well G1) than with TOC content ( $R^2 = 0.59$  for samples from wells G2 and G3;  $R^2 = 0.56$  for samples from well G1) (Fig. 12(b) and (c)). These



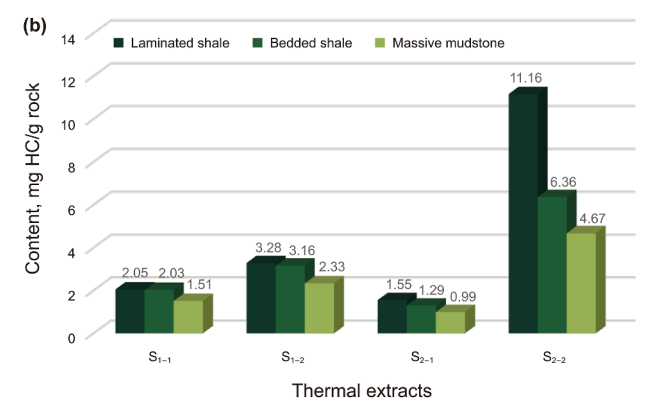
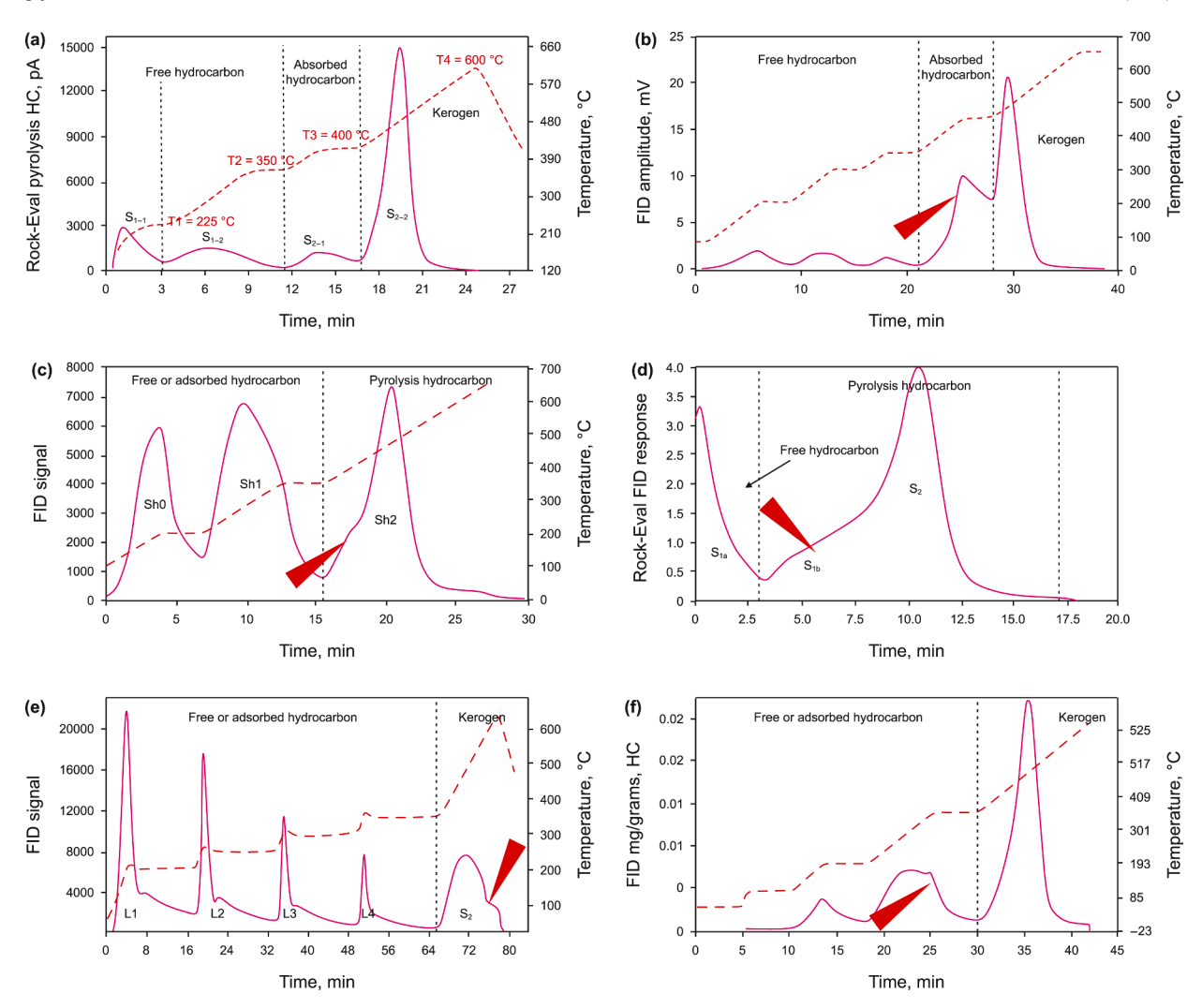


Fig. 9. Average thermal extracts content of shales with different lithologies (a) and different sedimentary structures (b).



**Fig. 10.** The diagram of multi-step programmed pyrolysis method (the arrow points to "shoulder"). (a) The Rock-Eval pyrogram generated by Ek<sub>2</sub> shales. (b) Modified from Li et al. (2020a). (c) Modified from Romero-Sarmiento (2019). (d) Modified from Li et al. (2020c). (e) Modified from Gentzis et al. (2021). (f) Modified from Maende et al. (2017).



**Fig. 11.** Compositions of light-to-medium n-alkanes of freshly extracted crude oil and thermal extracts (below 225  $^{\circ}$ C).

findings highlight kerogen's crucial role in controlling adsorbed oil content.

The oil adsorption capacity of kerogen in the Jiyang Depression is approximately 142 mg/g (Wang et al., 2019). Swelling experiments and theoretical calculations indicate that Type I and Type II $_1$  kerogen have an oil adsorption capacity of 120–150 mg/g (Tian et al., 2014; Wei et al., 2012). The adsorption and swelling capacities of kerogen vary among different types due to structural

differences. Type I kerogen exhibits a stronger adsorption and swelling capacities than Type II<sub>1</sub> at  $R_0$  ranging from 0.5% to 0.9% (Tian et al., 2014). The TOC content, maturity, and maceral characteristics of G2 and G3 samples are similar (Table 1, Nos. 21–68); therefore, the samples from both wells were analyzed jointly. According to Fig. 12(b), the adsorbed oil content per unit mass of kerogen in wells G2 and G3 is 131 mg/g (green trend line). The adsorption capacity of kerogen in well G1 (142 mg/g) is comparable to that of shale from the Shahejie Formation in the Jiyang Depression of the Bohai Bay Basin (Fig. 12(b); purple trend line) (Wang et al., 2019). The variation in kerogen adsorption capacity suggests that the oil adsorption capacity of kerogen decreases as thermal maturity increase.

#### 5.2.2. The effect of mineral compositions

The pyrolysis S<sub>1-1</sub>, S<sub>1-2</sub>, S<sub>2-1</sub>, and S<sub>2-2</sub> values of felsic shales are notably high (Fig. 9(a)). A linear relationship is observed between felsic mineral content and TOC content (Zhao et al., 2019). Felsic and organic-rich laminae couplets are commonly developed in felsic shale (Fig. 5(a) and (b)). The strong association between high felsic mineral content and elevated TOC content can be attributed to the influx of terrigenous clastic material, which brought in significant nutrients and triggered algal blooms in the lake (Zhao

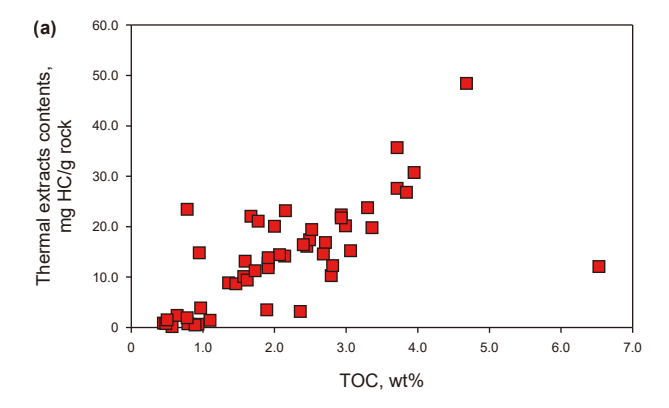
et al., 2019). However, no significant correlation is observed between mineral content and adsorbed oil content. The oil adsorption capacity of kerogen can exceed 130 mg/g, which is considerably higher than that of minerals in shale. Pernyeszi et al. (1998) reported that the oil adsorption capacities of illite and kaolinite were 33.9 mg/g and 17.1 mg/g, respectively. In particular, the oil adsorption capacities of quartz and carbonate minerals are lower than 2 mg/g (Daughney, 2000; Li et al., 2016), Although temperature, pressure, and particle size can influence mineral adsorption capacity (Ribeiro et al., 2009), it remains significantly lower than that of organic matter. To eliminate the influence of organic matter, the oil adsorption capacity of the three shale lithofacies (felsic, carbonate, and mixed shales) from wells G2 and G3 was determined by normalizing the content of adsorbed oil to TOC content. The adsorption capacities of the three lithofacies ranged from 0.56 to 0.57 mg HC/g TOC.

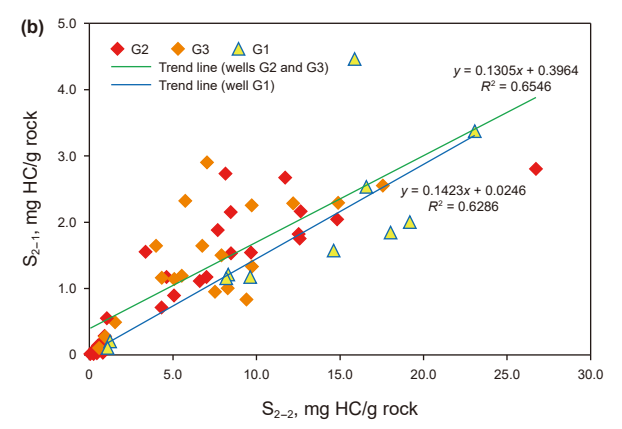
Free oil content is primarily influenced by the size of reservoir space. Felsic mineral particles exhibit strong resistance to compaction, and the relatively large intergranular pores preserved provide effective storage space for free oil (Fig. 5(b)). The processes of carbonate mineral dissolution, cementation, and recrystallization significantly impact shale reservoir quality (Bai et al., 2018). Calcite cementation and recrystallized minerals filled the primary pore space. Lower TOC content and reservoir densification are key factors contributing to the low oil content in carbonate shales (Fig. 5(e) and (f)).

#### 5.2.3. The effect of sedimentary structures

Sedimentary structure significantly influences the occurrence state of shale oil by controlling the distribution of original depositional organic matter, its interaction with minerals, the development of reservoir space, and the efficiency of hydrocarbon expulsion. Laminated shale, characterized by its high free oil content (Fig. 5(b)), is a key target for shale oil exploration and development (Zhao et al., 2019). In the Jiyang Depression of the Bohai Bay Basin in China, approximately 73% of shale oil production originates from laminated shale (Song et al., 2015). Similarly, a significant proportion of free oil has been identified in laminated shale within the Lucaogou Formation of the Junggar Basin (Wang, 2021). Felsic laminae predominantly form during the rainy season, corresponding with a significant influx of terrigenous clasts (Zhao et al., 2019; Deng et al., 2020). These felsic laminae are commonly found adjacent to organic-rich laminae (Fig. 5(a) and (b)), facilitating the migration of oil generated in organic-rich laminae to adjacent felsic laminae.

Due to the absence of sedimentary organic matter in felsic laminae (Fig. 5(b)), the oil within felsic laminae are primarily composed of migrated low-to-medium molecular weight hydrocarbons. During migration into adjacent felsic laminae, most high molecular weight components are retained in the organic-rich laminae, while mobile components such as aliphatic hydrocarbons preferentially migrated (Han et al., 2019). However, telalginite and lamalginite in organic-rich laminae exhibit strong shale oil adsorption properties. Additionally, the limited pore volume in organic-rich laminae restricts their ability to store free oil (Bao et al., 2016; Zhao et al., 2017; Wang et al., 2019). Consequently, felsic laminae predominantly contain free oil, while organic-rich laminae primarily consist of adsorbed oil (Jin et al., 2021a). The observations obtained using confocal laser scanning microscopy support this conclusion (Liu et al., 2021; Gao et al., 2023). Therefore, laminated felsic shale exhibits a notably higher movable oil content, with  $S_{1-1}$  values ranging from 1.37 to 2.85 mg HC/g rock and an average of 2.10 mg HC/g rock, which is higher than the average value of 1.87 mg HC/g rock in the Ek<sub>2</sub> shale. In contrast, massive mudstone exhibits greater homogeneity (Fig. 4





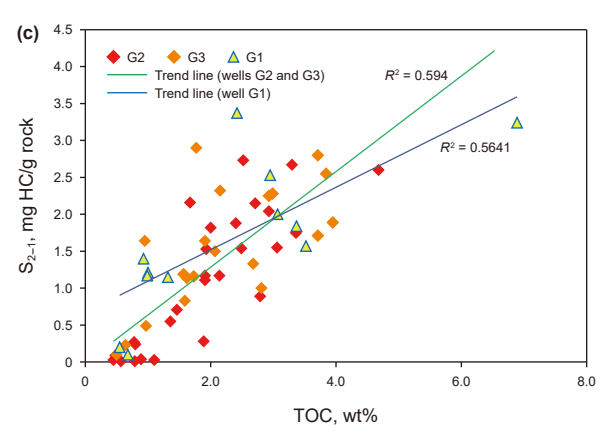


Fig. 12. Correlations between TOC content and thermal extracts content (a),  $S_{2-2}$  and  $S_{2-1}$  (b), TOC content and  $S_{2-1}$  (c).

(g)-(i); Fig. 5(c)), with clay minerals and calcite filling intergranular pores, reducing storage space and resulting in low oil content. Moreover, massive mudstone lacks the source-reservoir configuration found in laminated shales, which hinders the separation of shale oil in different occurrence states. Notably, laminae thickness significantly impacts fluid transport efficiency in shale (Liang et al., 2018). Zhang (2005) observed that the permeability ratio between parallel and vertical bedding directions in laminated shale can reach 32.3:1, while massive mudstone shows no obvious difference. Chen and Zha (2006) found that laminated shale retains free oil less efficiently than massive mudstone, as demonstrated by thermal simulation experiment showing efficient expulsion of free oil along bedding directions in laminated shale. In this study, good intergranular pore connectivity within felsic laminae is observed (Fig. 5(a) and (b)), which greatly enhances lateral permeability.

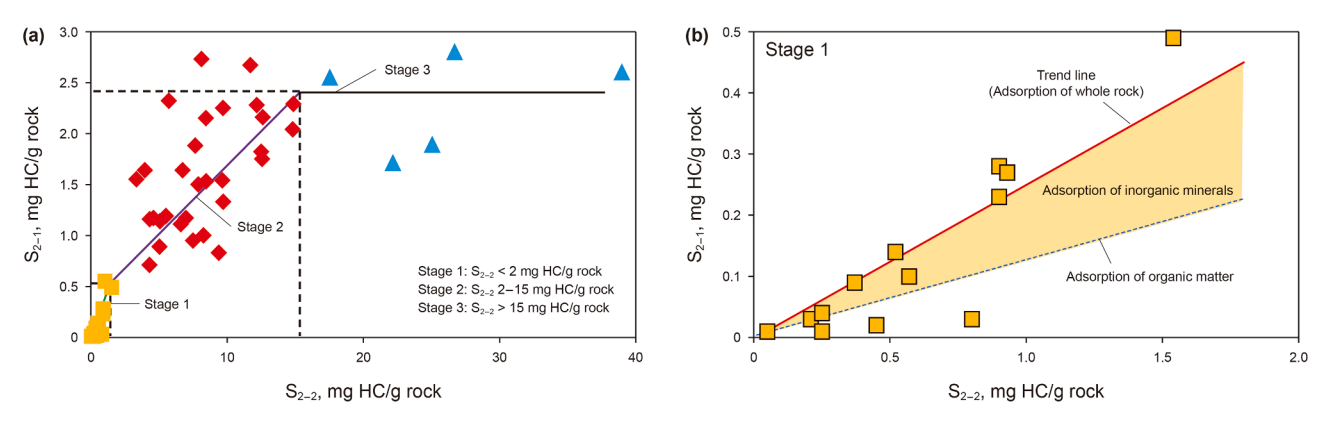


Fig. 13. Correlations between  $S_{2-2}$  and  $S_{2-1}$ . (a) A "trichotomy" correlation between  $S_{2-2}$  and  $S_{2-1}$ . (b) The stage 1 of (a).

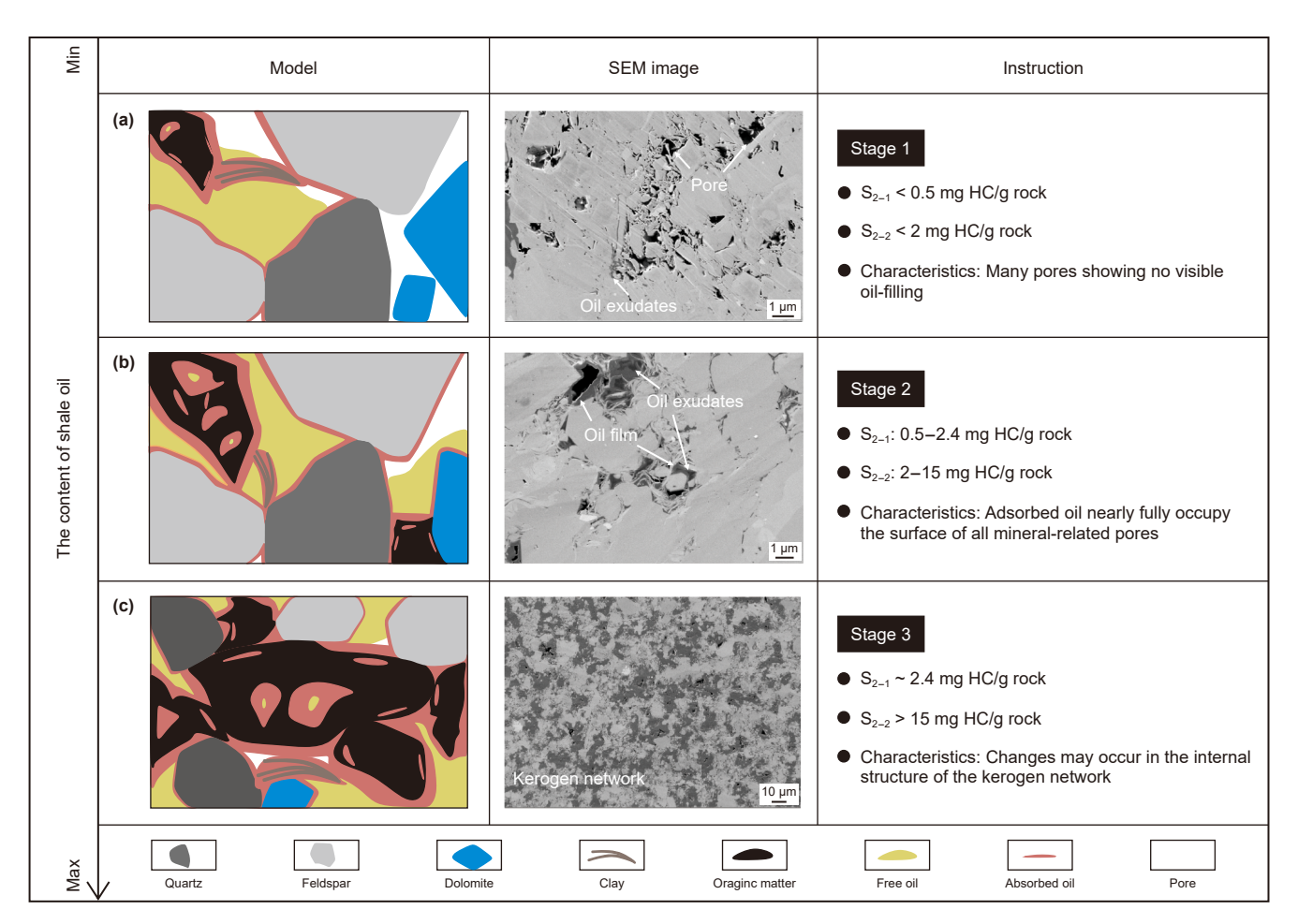


Fig. 14. A "trichotomy" occurrence model of shale oil.

# 5.3. Shale oil occurrence difference and potential evaluation

The adsorbed oil content is primarily controlled by the abundance of organic matter (Sandvik et al., 1992; Wei et al., 2012; Wang et al., 2019; Alafnan et al., 2020). In this study, the adsorbed oil content in well G2 and G3 exhibits a "trichotomy" correlation with  $S_{2-2}$  (Fig. 13), suggesting that its controlling factors may undergo stage-wise changes.

In stage 1,  $S_{2-2} < 2$  mg HC/g rock and  $S_{2-1} < 0.5$  mg HC/g rock, the low organic matter content results in low oil content, with

many pores showing no visible oil-filling (Fig. 14(a)). However, the generated oil had already satisfied kerogen adsorption and began migrating outward at this maturity. When oil filled mineral-related pores, it predominantly existed in an adsorbed state on the mineral surface (Wang, 2021). The joint adsorption by organic matter and minerals led to a rapid increase in the adsorbed oil content (Fig. 13(b)). In stage 2, where 2 mg HC/g rock < S2-2 < 15 mg HC/g rock and 0.5 mg HC/g rock < S2-1 < 2.4 mg HC/g rock, the adsorbed oil nearly fully occupied the surfaces of all mineral-related pores (Fig. 14(b)), and its content was primarily

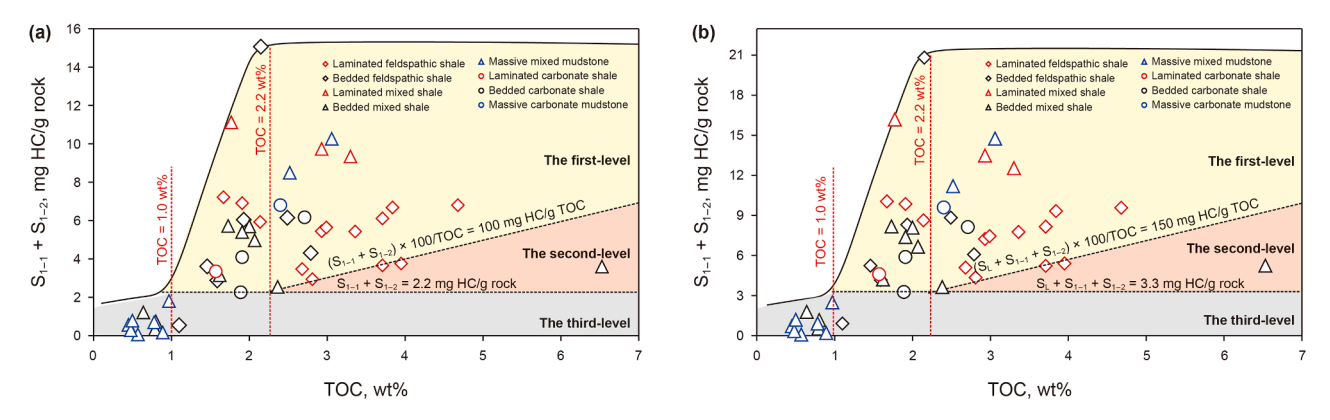


Fig. 15. The evaluation criteria of shale oil resources. (a) Before applying light hydrocarbon correction. (b) After applying light hydrocarbon correction.

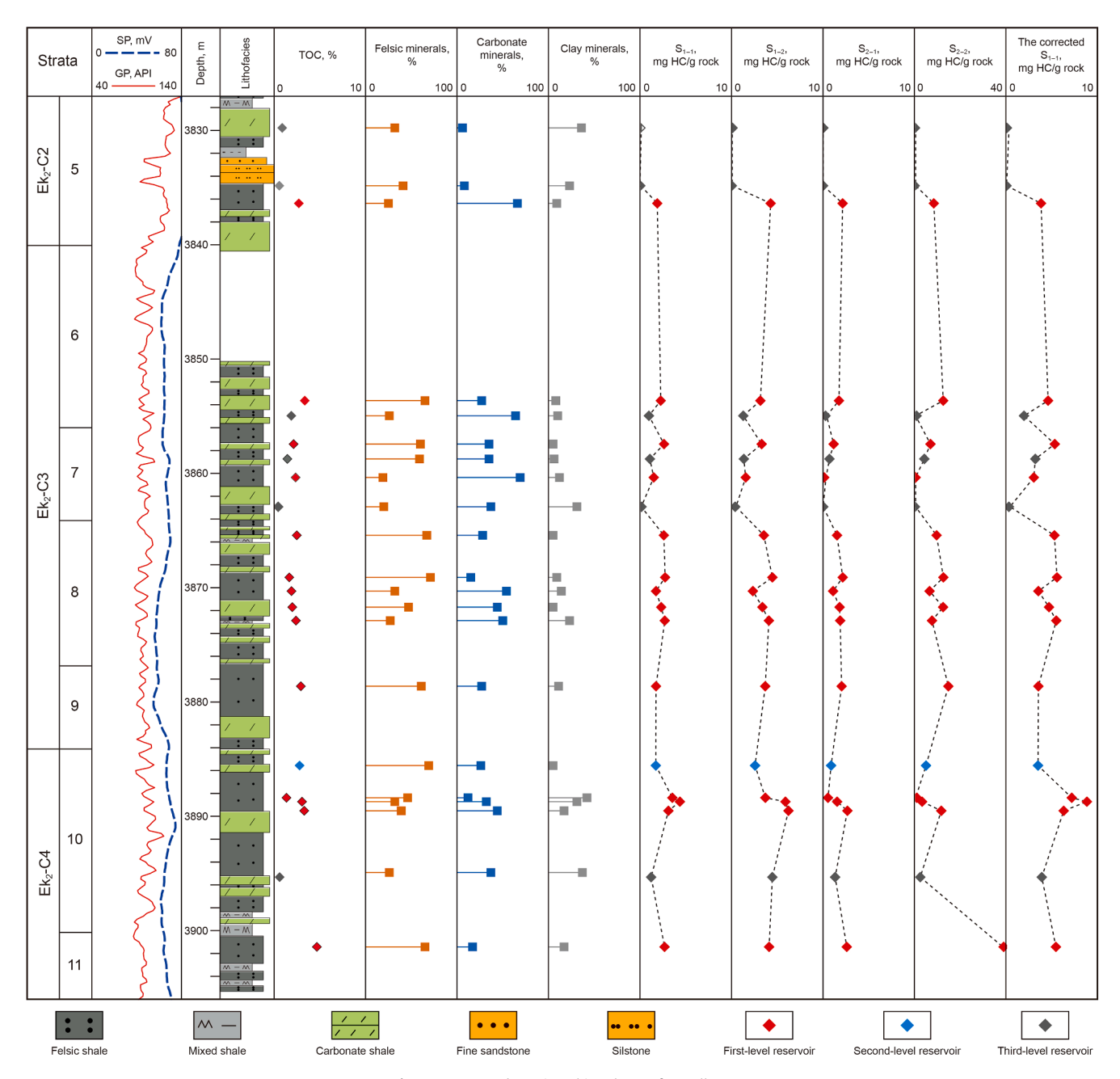


Fig. 16. Integrated stratigraphic columns for well G2.

controlled by the kerogen content. Therefore, the rate of increase in adsorbed oil content slowed with the increase in  $S_{2-2}$  (Fig. 13(a)). Based on the slope of the trend line, the adsorption capacity of kerogen for oil in the shale of wells G2 and G3 is estimated to be approximately 131 mg/g. By the end of the stage 1, kerogen had adsorbed 0.26 mg HC/g rock of oil (as indicated by the dashed trend line in Fig. 13(b)), while minerals had adsorbed 0.24 mg HC/g rock (the difference in the values represented by the red trend line and the dashed trend line in Fig. 13(b)). In stage 3, where  $S_{2-2}$  > 15 mg HC/g rock, as the kerogen content increases, the supportive effect of rigid minerals weakens (Fig. 14(c)). Under compaction, changes may occur in the internal structure of the kerogen network (Cardott et al., 2015), resulting in reduced adsorption sites. This could potentially explain the lack of a significant correlation between adsorbed oil content and kerogen content (Fig. 13 (a)).

Shale oil is generally classified into dispersed, inefficient, and enriched resources, based on the "trichotomy" correlation between pyrolysis S<sub>1</sub> and TOC content (Lu et al., 2012). A similar relationship between free oil content and TOC content is observed in samples

studied herein (Fig. 15(a)). When the TOC content is less than 1.0 wt %, the limited oil content cannot entirely fill the pores, and expelled oil from kerogen predominantly adheres to the mineral-related pore surfaces as adsorbed oil (Baruch et al., 2015; Misch et al., 2019), resulting in a relatively low free oil content. As organic matter content increases (1.0 wt% < TOC content < 2.2 wt%), mineral-related pores become nearly fully covered by oil films (Fig. 14(b)). At this stage, shale oil mainly accumulates in a free state, leading to a positive correlation between free oil content and TOC content. When TOC exceeds 2.2 wt%, the free oil content stabilizes at a high level, indicating that shale oil content has reached saturation and some excess oil is expelled. Thus, free oil content is primarily controlled by the storage capacity of shales. Consequently, when  $S_{1-1} + S_{1-2} > 2.2$  mg HC/g rock, a significant content of free oil accumulates, and when the TOC content exceeds 2.2 wt%, hydrocarbons begin to be expelled from the shale system.

The OSI method is widely used to evaluate shale oil potential in both marine and terrestrial sedimentary systems (Jarvie, 2012; Wang et al., 2015; Cao et al., 2017; Hu et al., 2021). Romero-Sarmiento et al. (2017) modified it into OSI =  $(Sh0 + Sh1) \times 100/$ 

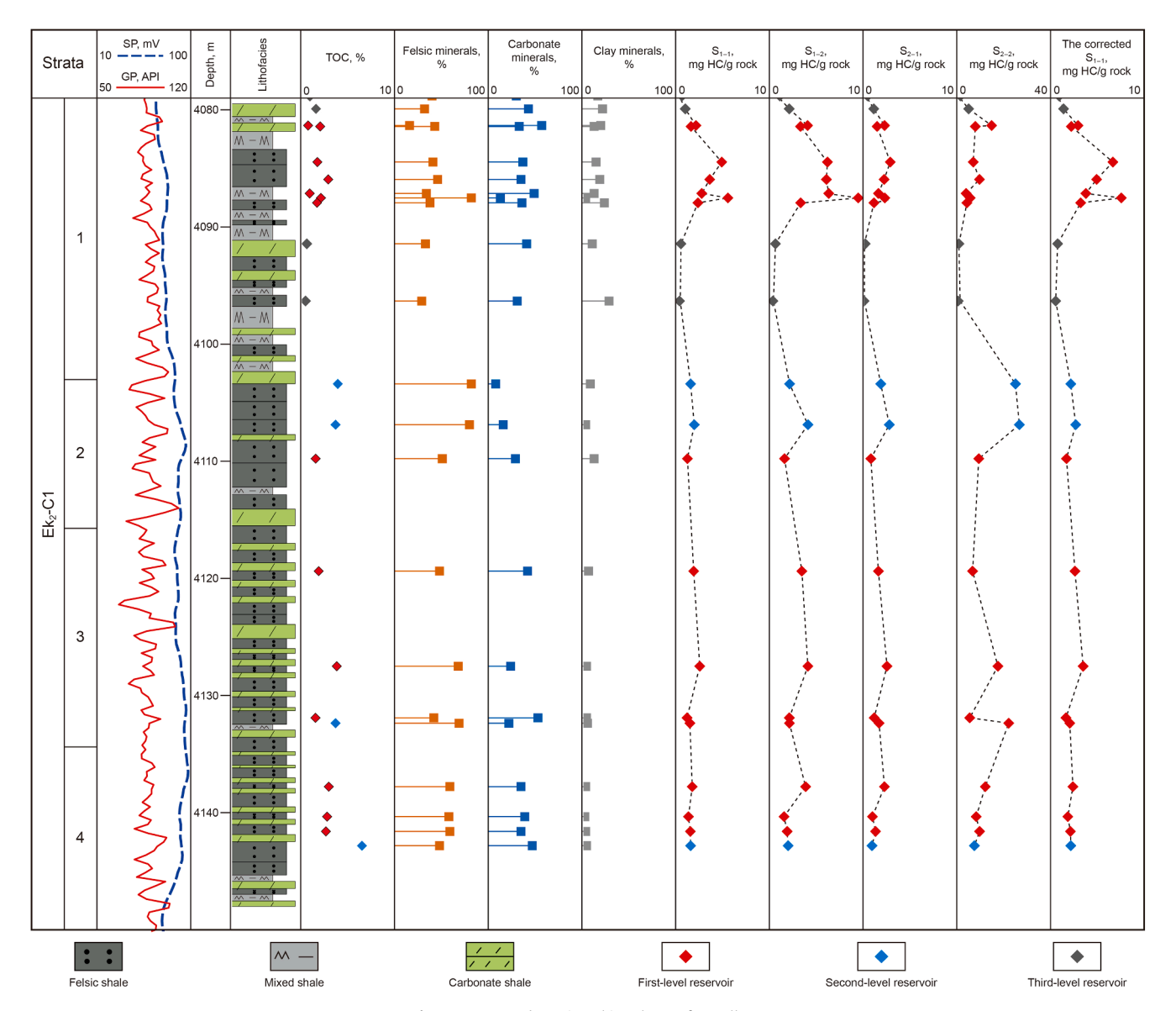


Fig. 17. Integrated stratigraphic columns for well G3.

TOC by employing multi-step programmed pyrolysis parameters. Compared to the traditional  $S_1 \times 100/TOC$  approach, this new method accounts for the influence of high molecular weight hydrocarbon components on oil saturation. However, the Sh0 and Sh1 peaks do not distinguish between free and adsorbed hydrocarbons (Romero-Sarmiento, 2019), and adsorbed hydrocarbons may not be considered in oil saturation evaluations under current technical conditions due to their immobility. In this study, adjusted pyrolysis scheme is used to differentiate between free oil and adsorbed oil. Therefore, using  $(S_{1-1} + S_{1-2}) \times 100/TOC$  as the evaluation criterion effectively avoids the influence of "solid-like" adsorbed oil.

A significant content of free oil accumulates when  $S_{1-1} + S_{1-2} >$ 2.2 mg HC/g rock (Fig. 13), and the TOC content of enriched resource is typically greater than 2.2% (Lu et al., 2012). The intersection of these values, expressed as  $(S_{1-1} + S_{1-2}) \times 100/$ TOC = 100 mg HC/g TOC, defines the threshold for shale oil extractability. Shales can be classified into three levels based on the values of  $S_{1-1} + S_{1-2}$  and  $(S_{1-1} + S_{1-2}) \times 100/TOC$  (Fig. 15(a)). First-level shales, characterized by  $S_{1-1} + S_{1-2} > 2.2$  mg HC/g rock and  $(S_{1-1} + S_{1-2}) \times 100/TOC > 100 \text{ mg HC/g TOC}$  (without correction of light hydrocarbons), possess significant commercial potential for shale oil extraction. Second-level shales, with  $S_{1-1} + S_{1-2} >$ 2.2 mg HC/g rock but (S $_{1-1}$  + S $_{1-2}$ )  $\times$  100/TOC < 100 mg HC/g TOC, have relatively low oil mobility but still hold development potential. Third-level shales, with  $S_{1-1} + S_{1-2} < 2.2$  mg HC/g rock, are challenging to exploit for shale oil (Fig. 15(a)). After applying light hydrocarbon correction, the threshold values for  $S_L + S_{1-1} + S_{1-2}$ and  $(S_L + S_{1\text{--}1} + S_{1\text{--}2}) \times 100/TOC$  are adjusted to 3.3 mg HC/g rock and 150 mg HC/g TOC, respectively (Fig. 15(b)). Overall, the Ek2 shale demonstrates significant exploitation potential, with the first-level reservoirs accounting for 66%, while second- and thirdlevel reservoirs comprise 11% and 23%, respectively (Fig. 15(a)). Notably, 85% of the laminated felsic shale is classified as first-level, making it a particularly favorable lithofacies for current exploration.

The mobility of shale oil is controlled by both the organic and inorganic characteristics of the shale (Wang et al., 2019). Although increasing TOC content enhances the abundance of free and adsorbed oil, excessive TOC content (>4.0 wt%) reduces oil mobility due to the strong adsorption capacity of organic matter (Jarvie, 2012). This is evidenced by the declining ( $S_{1-1} + S_{1-1}$  $_2) \times 100/TOC$  ratio (Fig. 15). Moderate TOC concentrations (2.0 wt %–4.0 wt%) in shale corresponds to the highest  $(S_{1-1}+S_{1-2}) \times 100/$ TOC ratios (100-700 mg HC/g TOC), indicating optimal producibility conditions (Fig. 15). In addition to organic characteristics, lithofacies exert a significant influence on oil mobility. As discussed in Section 5.2.3, the interbedding of organic-rich and felsic laminae provides favorable reservoir space for movable oil. Therefore, laminated felsic shales with moderate TOC content (2.0-4.0 wt%) are generally classified as first-level reservoirs (Fig. 15). These high-quality reservoirs are predominantly distributed in the 1st and 3rd sublayers of Ek2-C1 and the 8th sublayer of Ek<sub>2</sub>-C3, collectively accounting for over 70% of the total thickness (Figs. 16 and 17). This distribution is consistent with exploration practices (Han et al., 2021).

### 6. Conclusions

This study presents a novel multi-step pyrolysis method, combining pyrolysis-gas chromatography and crude oil gas chromatography, to systematically quantify the oil in different occurrence states in the lacustrine Ek<sub>2</sub> shales from the Cangdong Sag in the Bohai Bay Basin. The results indicate that laminated shales, particularly those with felsic laminae, are the most favorable

lithology for shale oil enrichment. The high-frequency alternation between organic-rich and felsic laminae forms a "source-reservoir" configuration that enhances shale oil accumulation. Additionally, a "trichotomy" correlation is observed between free/ adsorbed oil content and TOC content/S<sub>2-2</sub>, revealing that different mechanisms govern the occurrence of shale oil at distinct stages. Oil generated from kerogen must first satisfy its adsorption capacity before filling mineral-related pores, with the oil in contact with the mineral surfaces primarily existing in an adsorbed state. Based on these findings, we propose that shales with  $S_{1-1} + S_{1-2} >$ 2.2 mg HC/g rock and  $(S_{1-1} + S_{1-2}) \times 100/TOC > 100$  mg HC/g TOC are most likely to have significant commercial potential for shale oil extraction. The integration of free oil and TOC contents offers a more reliable method for evaluating shale oil potential, effectively excluding low-quality resources with high mobility or high TOC content, and overcoming the limitations of conventional OSI and "trichotomy" evaluation methods proposed by previous studies.

#### **CRediT authorship contribution statement**

Zhi-Hao Wang: Writing – original draft, Methodology, Investigation. Jian-Hua Zhao: Resources, Writing – review & editing, Project administration, Validation, Data curation. Xian-Zheng Zhao: Resources, Supervision. Ke-Yu Liu: Writing – review & editing, Funding acquisition. Xiu-Gang Pu: Resources. Qin-Hong Hu: Writing – review & editing, Funding acquisition. Wen-Zhong Han: Resources. Wei Zhang: Resources. Zhan-Nan Shi: Resources.

#### **Declaration of competing interest**

The authors declare that they have no known competing financial interests or personal relationships that could have appeared to influence the work reported in this paper.

#### Acknowledgements

This research was supported by the National Natural Science Foundation of China (No. 41830431), the Shandong Provincial Key Research and Development Program (No. 2020ZLYS08). We express our gratitude for the information and samples provided by Dagang Oilfield Company. We further thank Wuxi Research Institute of Petroleum Geology for the technical support.

#### Appendix A. Supplementary data

Supplementary data to this article can be found online at https://doi.org/10.1016/j.petsci.2025.07.001.

#### References

Alafnan, S., Solling, T., Mahmoud, M., 2020. Effect of kerogen thermal maturity on methane adsorption capacity: a molecular modeling approach. Molecules 25 (16), 3764. https://doi.org/10.3390/molecules25163764.

Ambrose, R.J., Hartman, R.C., Diaz-Campos, M., et al., 2012. Shale gas-in-place calculations part I: new pore-scale considerations. SPE J. 17 (1), 219–229. https://doi.org/10.2118/131772-PA.

Bai, C.Y., Yu, B.S., Liu, H.M., et al., 2018. The genesis and evolution of carbonate minerals in shale oil formations from Dongying Depression, Bohai Bay Basin, China. Int. J. Coal Geol. 189, 8–26. https://doi.org/10.1016/j.coal.2018.02.008.

Bao, Y.S., Zhang, L.Y., Zhang, J.G., et al., 2016. Factors influencing mobility of Paleogene shale oil in Dongying Sag, Bohai Bay Basin. Oil Gas Geol. 37 (3), 408–414 (in Chinese). https://doi.org/10.11743/ogg20160314.

Baruch, E.T., Kennedy, M.J., Löhr, S.C., et al., 2015. Feldspar dissolution-enhanced porosity in Paleoproterozoic shale reservoir facies from the barney creek formation (McArthur Basin, Australia). AAPG (Am. Assoc. Pet. Geol.) Bull. 99 (9), 1745–1770. https://doi.org/10.1306/04061514181.

Behar, F., Kressmann, S., Rudkiewicz, J.L., et al., 1992. Experimental simulation in a confined system and kinetic modelling of kerogen and oil cracking. Org. Geochem. 19 (1–3), 173–189. https://doi.org/10.1016/0146-6380(92)90035-V.

- Behar, F., Vandenbroucke, M., Tang, Y., et al., 1997. Thermal cracking of kerogen in open and closed systems: determination of kinetic parameters and stoichiometric coefficients for oil and gas generation. Org. Geochem. 26 (5–6), 321–339. https://doi.org/10.1016/S0146-6380(97)00014-4.
- Beti, D.R., Panja, P., Jiang, C.Q., et al., 2020. Change in hydrocarbon composition in rock samples as a function of time: a thermodynamic evaporation model. J. Nat. Gas Sci. Eng. 77, 103238. https://doi.org/10.1016/j.jngse.2020.103238.
- Cady, W.E., Seelig, H.S., 1952. Composition of shale oil. Ind. Eng. Chem. 44 (1), 2636–2641. https://doi.org/10.1021/ie50515a044.
- Cao, H.R., Zou, Y.R., Lei, Y., et al., 2017. Shale oil assessment for the Songliao Basin, Northeastern China, using oil generation sorption method. Energy Fuels 31 (5), 4826–4842. https://doi.org/10.1021/acs.energyfuels.7b00098.
- Cardott, B.J., Landis, C.R., Curtis, M.E., 2015. Post-oil solid bitumen network in the Woodford shale, USA—A potential primary migration pathway. Int. J. Coal Geol. 139, 106–113. https://doi.org/10.1016/j.coal.2014.08.012.
   Centurion, S., Cade, R., Luo, X.L., et al., 2013. Eagle ford shale: hydraulic fracturing,
- Centurion, S., Cade, R., Luo, X.L., et al., 2013. Eagle ford shale: hydraulic fracturing, completion and production trends, part III. In: SPE Annual Technical Conference and Exhibition. Onepetro. https://doi.org/10.2118/166494-MS.
- Chen, Z.H., Zha, M., 2006. Simulation experiment of geological color layer effect of source rock. Geochimica 35 (2), 157–166 (in Chinese). https://doi.org/10.19700/i.0379-1726.2006.02.006.
- Collell, J., Ungerer, P., Galliero, G., et al., 2014. Molecular simulation of bulk organic matter in type II shales in the middle of the oil formation window. Energy Fuels 28 (12), 7457–7466. https://doi.org/10.1021/ef5021632.
- Cooles, G.P., Mackenzie, A., Quigley, T.M., 1986. Calculation of petroleum masses generated and expelled from source rocks. Org. Geochem. 10 (1–3), 235–245. https://doi.org/10.1016/0146-6380(86)90026-4.
- Daughney, C.J., 2000. Sorption of crude oil from a non-aqueous phase onto silica: the influence of aqueous pH and wetting sequence. Org. Geochem. 31 (2–3), 147–158. https://doi.org/10.1016/S0146-6380(99)00130-8.
- Deng, Y., Chen, S.Y., Pu, X.G., et al., 2020. Formation mechanism and environmental evolution of fine-grained sedimentary rocks from the second member of Kongdian formation in the Cangdong Sag, Bohai Bay Basin. Oil Gas Geol. 41 (4), 811–823, 890 (in Chinese). https://doi.org/10.11743/ogg20200414.
- Dou, Y., Han, W.Z., Wang, W.D., et al., 2024. Assessment of movable resources of lacustrine shale oil based on mass oil content: a case study of the 2nd member of Kongdian formation in Cangdong Sag of the Bohai Bay Basin. Journal of Shenzhen University Science & Engineering 41 (1), 33–41 (in Chinese). https://doi.org/10.3724/SP.J.1249.2024.01033.
- Espitalie, J., Deroo, G., Marquis, F., 1986. La pyrolyse Rock-Eval et ses applications. Troisième partie. Rev. Inst. Fr. Petrol 41 (1), 73–89. https://doi.org/10.2516/ogst:1986003.
- Espitalie, J., Laporte, J.L., Madec, M., et al., 1977. Méthode rapide de caractérisation des roches mètres, de leur potentiel pétrolier et de leur degré d'évolution. Oil Gas Sci. Technol. 32, 23–42. https://doi.org/10.2516/ogst:1977002.
- Feng, Y., Xiao, X.M., Wang, E., et al., 2021. Oil retention in shales: a review of the mechanism, controls and assessment. Front. Earth Sci. 9, 720839. https://doi.org/10.3389/feart.2021.720839.
- Fleury, M., Romero-Sarmiento, M.F., 2016. Characterization of shales using T1–T2 NMR maps. J. Petrol. Sci. Eng. 137, 55–62. https://doi.org/10.1016/j.petrol. 2015.11.006.
- Gao, Z.Y., Duan, L.F., Jiang, Z.X., et al., 2023. Using laser scanning confocal microscopy combined with saturated oil experiment to investigate the pseudo insitu occurrence mechanism of light and heavy components of shale oil in sub-micron scale. J. Petrol. Sci. Eng. 220, 111234. https://doi.org/10.1016/j.petrol.2022.111234.
- Gentzis, T., Carvajal-Ortiz, H., Xie, Z.H., et al., 2021. An integrated geochemical, spectroscopic, and petrographic approach to examining the producibility of hydrocarbons from liquids-rich unconventional formations. Fuel 298, 120357. https://doi.org/10.1016/j.fuel.2021.120357.
- Han, W.Z., Zhao, X.Z., Jin, F.M., et al., 2021. Sweet spot evaluation and exploration practice of lacustrine shale oil of the second member of Kongdian formation in Cangdong sag, Bohai Bay Basin. Petrol. Explor. Dev. 48 (4), 900–910. https://doi.org/10.1016/S1876-3804/21)60075-7
- Han, Y.J., Horsfield, B., LaReau, H., et al., 2019. Intraformational migration of petroleum: insights into the development of sweet spot in the Cretaceous Niobrara shale-oil system, Denver Basin. Mar. Petrol. Geol. 107, 301–309. https://doi.org/10.1016/j.marpetgeo.2019.05.026.
- Hu, T., Pang, X.Q., Jiang, F.J., et al., 2021. Movable oil content evaluation of lacustrine organic-rich shales: methods and a novel quantitative evaluation model. Earth Sci. Rev. 214, 103545. https://doi.org/10.1016/j.earscirev.2021.103545.
- Inan, S., Yalçin, M.N., Mann, U., 1998. Expulsion of oil from petroleum source rocks: inferences from pyrolysis of samples of unconventional grain size. Org. Geochem. 29, 45–61. https://doi.org/10.1016/S0146-6380(98)00091-6.
- Jarvie, D.M., 2012. Shale resource systems for oil and gas: part 2—Shale-oil resource systems. In: Breyer, J.A. (Ed.), Shale reservoirs—Giant Resources for the 21st Century, vol. 97. AAPG Memoir, pp. 89–119. https://doi.org/10.1306/13321447M973489
- Jarvie, D.M., Hill, R.J., Ruble, T.E., et al., 2007. Unconventional shale-gas systems: the Mississippian Barnett Shale of north-central Texas as one model for thermogenic shale-gas assessment. AAPG (Am. Assoc. Pet. Geol.) Bull. 91 (4), 475–499. https://doi.org/10.1306/12190606068.
- Jiang, Q.G., Li, M.W., Qian, M.H., et al., 2016. Quantitative characterization of shale oil in different occurrence states and its application. Petroleum Geology &

- Experiment 38 (6), 842–849 (in Chinese). https://doi.org/10.11781/sysydz201606842.
- Jin, Z.J., Wang, G.P., Liu, G.X., et al., 2021a. Research progress and key scientific issues of continental shale oil in China. Acta Pet. Sin. 42 (7), 821–835 (in Chinese). https://doi.org/10.7623/syxb202107001.
- Jin, Z.J., Zhu, R.K., Liang, X.P., et al., 2021b. Several issues worthy of attention in current lacustrine shale oil exploration and development. Petrol. Explor. Dev. 48 (6), 1276–1287. https://doi.org/10.1016/S1876-3804(21)60303-8.
- Katz, B., Lin, F., 2014. Lacustrine basin unconventional resource plays: key differences. Mar. Petrol. Geol. 56, 255–265. https://doi.org/10.1016/j.marpetgeo.2014.02.013. Ko, L.T., Ruppel, S.C., Loucks, R.G., et al., 2018. Pore-types and pore-network evo-
- Ko, L.T., Ruppel, S.C., Loucks, R.G., et al., 2018. Pore-types and pore-network evolution in upper devonian-lower Mississippian woodford and Mississippian barnett mudstones: insights from laboratory thermal maturation and organic petrology. Int. J. Coal Geol. 190, 3–28. https://doi.org/10.1016/j.coal.2017.10.001.
- Lewan, M.D., 1985. Evaluation of petroleum generation by hydrous phrolysis experimentation. Phil. Trans. Roy. Soc. Lond. Math. Phys. Sci. 315 (1531), 123–134. https://doi.org/10.1098/rsta.1985.0033.
- Liang, C., Cao, Y.C., Liu, K.Y., et al., 2018. Diagenetic variation at the lamina scale in lacustrine organic-rich shales: implications for hydrocarbon migration and accumulation. Geochem. Cosmochim. Acta 229, 112–128. https://doi.org/10.1016/j.gca.2018.03.017.
- Liang, T., Zou, Y.R., Zhan, Z.W., 2021. Chemical struc.ture changes of solid bitumen during solvent swelling investigated by X-ray diffraction. Int. J. Coal Geol. 243, 103778. https://doi.org/10.1016/j.coal.2021.103778.
- Li, J.B., Jiang, C.Q., Wang, M., et al., 2020a. Adsorbed and free hydrocarbons in unconventional shale reservoir: a new insight from NMR T<sub>1</sub>-T<sub>2</sub> maps. Mar. Petrol. Geol. 116, 104311. https://doi.org/10.1016/j.marpetgeo.2020.104311.
- Li, J.B., Lu, S.F., Chen, G.H., et al., 2016. Correction of light and heavy hydrocarbon loss for residual hydrocarbon S<sub>1</sub> and its significance to assessing resource potential of E2s4(2) member in damintun sag. Bohai Bay Basin. Oil & Gas Geology. 37 (4), 538–545 (in Chinese). https://doi.org/10.11743/ogg20160410.
- Liu, B., Sun, J.H., Zhang, Y.Q., et al., 2021. Reservoir space and enrichment model of shale oil in the first member of Cretaceous Qingshankou formation in the Changling Sag, southern Songliao Basin, NE China. Petrol. Explor. Dev. 48 (3), 608–624. https://doi.org/10.1016/S1876-3804(21)60049-6.
- Li, Y., Liu, K.Y., Pu, X.G., et al., 2020b. Lithofacies characteristics and formation environments of mixed fine-grained sedimentary rocks in second member of kongdian formation in cangdong depression, Bohai Bay Basin. Earth Sci. 45 (10), 3779–3796 (in Chinese). https://doi.org/10.3799/dqkx.2020.167.
- Li, M.W., Chen, Z.H., Qian, M.H., et al., 2020c. What are in pyrolysis S<sub>1</sub> peak and what are missed? Petroleum compositional characteristics revealed from programed pyrolysis and implications for shale oil mobility and resource potential. Int. J. Coal Geol. 217, 103321. https://doi.org/10.1016/j.coal.2019.103321.
- Lu, S.F., 1996. The Theory of Organic Hydrocarbon Kinetics and its Applications. Petroleum Industry Press, Beijing (in Chinese).
- Lu, S.F., Huang, W.B., Chen, F.W., et al., 2012. Classification and evaluation criteria of shale oil and gas resources: discussion and application. Petrol. Explor. Dev. 39 (2), 268–276. https://doi.org/10.1016/S1876-3804(12)60042-1.
- Lu, S.F., Xue, H.T., Wang, M., et al., 2016. Several key issues and research trends in evaluation of shale oil. Acta Pet. Sin. 37 (10), 1309–1322 (in Chinese). https:// doi.org/10.7623/syxb201610012.
- Ma, D.H., Geng, C.X., Zuo, T.Q., 2005. Method of improving calculation accuracy of oil saturation. Pet. Geol. Oilfield Dev. Daqing 24 (2), 41–42 (in Chinese).
- Ma, W.J., Cao, Y.C., Xi, K.L., et al., 2023. The effect of lamina and lithofacies assemblage on molecular maturity of oil in a shale source-rock reservoir. Int. J. Coal Geol. 279, 104373. https://doi.org/10.1016/j.coal.2023.104373.
- Maende, A., Pepper, A., Jarvie, D.M., et al., 2017. Advanced pyrolysis data and interpretation methods to identify unconventional reservoir sweet spots in fluid phase saturation and fluid properties (API gravity) from drill cuttings and cores. Petroleum Geology 12 (4), 417-452. https://www.searchanddiscovery.com/pdfz/documents/2017/80596maende/ndx\_maende.pdf.html.
- McIver, R.D., 1967. Composition of kerogen-clue to its role in the origin of petroleum. In: 7th World Petroleum Congress. Onepetro.
- Merrill, R.K., 1991. Source and Migration Processes and Evaluation Techniques.

  American Association of Petroleum Geologists. https://doi.org/10.1306/ TrHbk543.
- Michael, G.E., Packwood, J., Holba, A., 2013. Determination of in-situ hydrocarbon volumes in liquid rich shale plays. In: Unconventional Resources Technology Conference. https://doi.org/10.1190/urtec2013-211.
- Misch, D., Gross, D., Hawranek, G., et al., 2019. Solid bitumen in shales: petrographic characteristics and implications for reservoir characterization. Int. J. Coal Geol. 205, 14–31. https://doi.org/10.1016/j.coal.2019.02.012.
- Pernyeszi, T., Patzkó, Á., Berkesi, O., et al., 1998. Asphaltene adsorption on clays and crude oil reservoir rocks. Colloids Surf. A Physicochem. Eng. Asp. 137 (1–3), 373–384. https://doi.org/10.1016/S0927-7757(98)00214-3.
- Peters, K.E., 1986. Guidelines for evaluating petroleum source rock using programmed pyrolysis. AAPG Bull. 70, 318–329. https://doi.org/10.1306/94885688-1704-11D7-8645000102C1865D.
- Pu, X.G., Zhou, L.H., Han, W.Z., et al., 2016. Geologic features of fine-grained facies sedimentation and tight oil exploration: a case from the second member of Paleogene Kongdian formation of Cangdong sag, Bohai Bay Basin. Petrol. Explor. Dev. 43 (1), 26–35. https://doi.org/10.1016/S1876-3804(16)30003-9.
- Qian, M.H., Jiang, Q.G., Li, M.W., et al., 2017. Quantitative characterization of extractable organic matter in lacustrine shale with different occurrences.

- Petroleum Geology & Experiment 39 (2), 278–286 (in Chinese). https://doi.org/ 10.11781/svsvdz201702278
- Rasdi, F., Chu, L., 2012. Diagnosing fracture network pattern and flow regime aids production performance analysis in unconventional oil reservoirs. In: SPE/ EAGE European Unconventional Resources Conference and Exhibition. One-Petro. https://doi.org/10.3997/2214-4609-pdb.285.spe151623.
- Ribeiro, R.C., Correia, J.C.G., Seidl, P.R., 2009. The influence of different minerals on the mechanical resistance of asphalt mixtures. J. Petrol. Sci. Eng. 65 (3–4), 171–174. https://doi.org/10.1016/j.petrol.2008.12.025.
- Romero-Sarmiento, M.F., 2019. A quick analytical approach to estimate both free versus sorbed hydrocarbon contents in liquid-rich source rocks. AAPG (Am. Assoc. Pet. Geol.) Bull. 103 (9), 2031–2043. https://doi.org/10.1306/02151918152.
- Romero-Sarmiento, M.F., Euzen, T., Rohais, S., et al., 2016. Artificial thermal maturation of source rocks at different thermal maturity levels: application to the Triassic Montney and Doig Formations in the Western Canada sedimentary Basin. Org. Geochem. 97, 148–162. https://doi.org/10.1016/j.orggeochem. 2016.05.002.
- Romero-Sarmiento, M.F., Letort, D., Pillot, D., et al., 2014. New Rock-Eval method for characterization of shale plays. 14<sup>th</sup> Latin American Congress on Organic Geochemistry, Buzios, Rio De Janeiro, Brazil. https://www.researchgate.net/publication/265550264.
- Romero-Sarmiento, M.F., Ramiro-Ramirez, S., Berthe, G., et al., 2017. Geochemical and petrophysical source rock characterization of the Vaca Muerta Formation, Argentina. Implications for unconventional petroleum resource estimations. Int. J. Coal Geol. 184, 27–41. https://doi.org/10.1016/j.coal.2017.11.004. Sandvik, E.I., Young, W.A., Curry, D.J., 1992. Expulsion from hydrocarbon sources:
- Sandvik, E.I., Young, W.A., Curry, D.J., 1992. Expulsion from hydrocarbon sources: the role of organic absorption. Org. Geochem. 19 (1–3), 77–87. https://doi.org/ 10.1016/0146-6380(92)90028-V.
- Song, G.Q., Xu, X.Y., Li, Z., et al., 2015. Factors controlling oil production from Paleogene shale in Jiyang depression. Oil Gas Geol. 36 (3), 463–471. https://doi.org/10.11743/ggg20150315.
- Sonnenberg, S.A., Pramudito, A., 2009. Petroleum geology of the giant Elm Coulee field, Williston Basin. AAPG Bull. 93 (9), 1127–1153. https://doi.org/10.1306/05280909006.
- Teerman, S.C., Hwang, R.J., 1991. Evaluation of the liquid hydrocarbon potential of coal by artificial maturation techniques. Org. Geochem. 17 (6), 749–764. https://doi.org/10.1016/0146-6380(91)90019-G.
- Tian, S.S., Xue, H.T., Lu, S.F., et al., 2014. Discussion on the mechanism of different types of kerogen remaining oil and gas. In: Annual Meeting of Chinese Geoscience Union, Beijing (in Chinese).
- Vandenbroucke, M., Largeau, C., 2007. Kerogen origin, evolution and structure. Org. Geochem. 38 (5), 719–833. https://doi.org/10.1016/j.orggeochem.2007.01.001.
- Wang, M., Ma, R., Li, J.B., et al., 2019. Occurrence mechanism of lacustrine shale oil in the Paleogene Shahejie Formation of Jiyang Depression, Bohai Bay Basin,

- China. Petrol. Explor. Dev. 46 (4), 789–802. https://doi.org/10.1016/S1876-3804
- Wang, M., Sherwood, N., Li, Z.S., et al., 2015. Shale oil occurring between salt intervals in the Dongpu depression, Bohai Bay Basin, China. Int. J. Coal Geol. 152, 100–112. https://doi.org/10.1016/j.coal.2015.07.004.
- Wang, S.Z., 2021. Lithofacies types and shale-oil accumulating characteristics of middle Permian Lucaogou formation in bogda area of Junggar Basin. Pet. Geol. Oilfield Dev. Daqing 40 (1), 16 (in Chinese). https://doi.org/10.19597/J. ISSN.1000-3754.201912017.
- Wei, Z.F., Zou, Y.R., Cai, Y.L., et al., 2012. Kinetics of oil group-type generation and expulsion: an integrated application to Dongying depression, Bohai Bay Basin, China. Org. Geochem. 52, 1–12. https://doi.org/10.1016/j.orggeochem.2012. 08.006
- Yang, R.C., Jin, Z.J., van Loon, T., et al., 2017. Climatic and tectonic controls of lacustrine hyperpycnite origination in the Late Triassic Ordos Basin, central China: implications for unconventional petroleum development. AAPG (Am. Assoc. Pet. Geol.) Bull. 101 (1), 95–117. https://doi.org/10.1306/06101615095.
- Zhang, L.Y., 2005. Reconsideration of hydrocarbon generation by "enriching organic matter": a case study of dongying depression. Geochimica 34 (6), 81–87 (in Chinese). https://doi.org/10.19700/j.0379-1726.2005.06.009.
- Zhang, P.F., Lu, S.F., Lin, Z.Z., et al., 2022. Key oil content parameter correction of shale oil resources: a case study of the Paleogene Funing Formation, Subei Basin, China. Energy Fuels 36 (10), 5316–5326. https://doi.org/10.1021/acs.energyfuels.2c00610
- Zhao, J.H., Jin, Z.J., Hu, Q.H., et al., 2017. Integrating SANS and fluid-invasion methods to characterize pore structure of typical American shale oil reservoirs. Sci. Rep. 7 (1), 1–16. https://doi.org/10.1038/s41598-017-15362-0.
- Zhao, X.Z., Jin, F.M., Pu, X.G., et al., 2024. Concentric hydrocarbon accumulations in deep rift basins: a case study of Jizhong and Huanghua depressions, Bohai Bay Basin, China. AAPG (Am. Assoc. Pet. Geol.) Bull. 2024 (108), 1387–1410. https://doi.org/10.1306/12052322018.
- Zhao, X.Z., Pu, X.G., Yan, J.H., et al., 2023. Cycles of fine-grained sedimentation and their influences on organic matter distribution in the second member of Paleogene Kongdian formation in Cangdong Sag, Bohai Bay Basin, East China. Petrol. Explor. Dev. 50 (3), 534–546. https://doi.org/10.1016/S1876-3804(23) 60408-2.
- Zhao, X.Z., Zhou, L.H., Pu, X.G., et al., 2019. Favorable formation conditions and enrichment characteristics of lacustrine facies shale oil in faulted lake basin: a case study of member 2 of Kongdian Formation in Cangdong sag, Bohai Bay Basin. Acta Petrol. Sin. 40 (9), 1013–1029 (in Chinese). https://doi.org/10.7626/ svxb201909001.
- Zou, C.N., Yang, Z., Cui, J.W., et al., 2013. Formation mechanism, geological characteristics and development strategy of nonmarine shale oil in China. Petrol. Explor. Dev. 40 (1), 14–26. https://doi.org/10.1016/S1876-3804(13)60002-6.